Squaramide-based supramolecular materials for 3D cell culture applications

Tong, C.

CHAPTER 2

Squaramide-based supramolecular materials for three-dimensional cell culture of human induced pluripotent stem cells and their derivatives

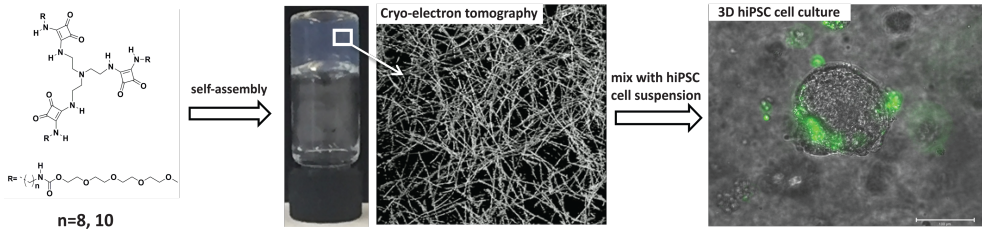

This chapter was published as an original research paper: Ciqing Tong, Tingxian Liu, Victorio Saez Talens, Willem E. M. Noteborn, Thomas H. Sharp, Marco M. R. M. Hendrix, Ilja K. Voets, Christine L. Mummery, Valeria V. Orlova, and Roxanne E. Kieltyka, *Biomacromolecules* **2018**, *19*, 1091-1099.

2.1 Abstract

The synthetic hydrogel materials can recapitulate the natural cell microenvironment; however, it is equally necessary that the gels maintain cell viability and phenotype while permitting reisolation without stress, especially for use in the stem cell field. Here, we describe a family of synthetically accessible, squaramide-based tripodal supramolecular monomers consisting of a flexible tris(2-aminoethyl)amine (TREN) core that self-assemble into supramolecular polymers and eventually into self-recovering hydrogels. Spectroscopic measurements revealed that monomer aggregation is mainly driven by a combination of hydrogen bonding and hydrophobicity. The self-recovering hydrogels were used to encapsulate NIH 3T3 fibroblasts as well as human-induced pluripotent stem cells (hiPSCs) and their derivatives in 3D. The materials reported here proved cytocompatible for these cell types with the maintenance of hiPSCs in their undifferentiated state essential for their subsequent expansion or differentiation into a given cell type and potential for facile release by dilution due to their supramolecular nature.

2.2 Introduction

The surging interest in adaptive materials for a broad range of applications, from biomedicine to electronics, has invigorated the development of functional materials within the supramolecular polymer community.[1-3] Because of their inherent noncovalent nature, supramolecular polymer materials can exhibit unique features in comparison to their covalent counterparts such as facile preparation, responsiveness, and self-healing. As biomaterials, their easy processing permits the mixing of numerous functionalized monomers with complex cargoes such as peptides, and their responsiveness to stimuli such as temperature, pH, light, and enzymes opens the door to designer materials that can deliver therapeutic cargo, or as scaffolds for 3D cell culture.[4-14] One particular area where supramolecular hydrogels can be especially useful is in the culture of human pluripotent stem cells (hPSCs), which are unique in their capacity to generate any body cell type. Human induced pluripotent stem cells (hiPSCs) have been shown to recapitulate all properties of human embryonic stem cells (hESCs) derived from preimplantation stage human embryos, but are instead derived from somatic cells obtained in a non-invasive manner by reprogramming with a set of transcription factors, thus overcoming ethical issues related to their embryonic counterparts.[15,16] Excitingly, hiPSCs have the potential for decreased immunogenicity because they can be derived from autologous sources, but they require specific culture conditions to maintain their pluripotent state.[17-20] To further enable their expansion and directed differentiation in 3D for applications such as drug screening, disease modeling, and eventually regenerative medicine, inert synthetic scaffolds and gentle release methods are required for optimal culture and recovery of the cells for further downstream applications.[21,22] However, to reach such end-stage applications in the biomedical area with supramolecular materials, structurally simple and biocompatible monomers with high synthetic accessibility that robustly self-assemble into polymeric architectures are necessary.

To promote supramolecular polymerization of a given monomer, a combination of noncovalent interactions such as hydrogen bonding, π-stacking, van der Waals and/or electrostatic interactions, are engineered into the monomer unit.[23-28] Hydrogen bonds are often employed because of their capacity to engender directional interactions between monomers while providing a handle to tune the strength of their association by their type, number, arrangement, and microenvironment.[29,30] Commonly used hydrogen bonding synthons include

amides,[31] thioamides,[32] ureas[33,34] and thioureas.[35] Despite their extensive use in the areas of bioconjugation,[36] medicinal chemistry,[37] catalysis,[38] and anion recognition,[39] squaramides have been explored to a far lesser extent in the materials domain, especially with respect to self-assembly,[39-41] with few examples reported in water,[42-44] and none thus far have been applied to 3D cell culture.

Squaramides are minimal ditopic hydrogen bonding units that possess two strong N−H hydrogen bond donors and two C=O hydrogen bond acceptors opposite one another on a conformationally rigid cyclobutenedione ring.[45] Their capacity to engage in strong hydrogen bonding interactions renders them as attractive building blocks to prepare noncovalent materials.[46] Previously, our group has demonstrated that these highly directional hydrogen bonding units can facilitate the formation of robust supramolecular polymers when incorporated into a bolaamphiphilic monomer benefiting from the interplay between hydrogen bonding and aromaticity in the squaramide unit.[42] We became interested in applying the squaramide synthon to a C3-type monomer geometry because of the possibilities for increased control over their self-assembly properties into one-dimensional aggregates.[47,48] On the basis of its commercial availability and structural simplicity, the flexible tripodal core tris(2-aminoethyl)amine (TREN)[49-53] was selected for coupling to the rigid squaramide unit so as to explore the self-assembly scope of this strong hydrogen bonding synthon. Thus, we report for the first time the synthesis of a library of flexible tripodal squaramide-based supramolecular polymer monomers and examine their self-assembly into supramolecular materials for applications in the 3D culture of hiPSCs and their derivatives.

2.3 Results and discussion

2.3.1 Tripodal squaramide-based amphiphile design and synthesis

A library of tripodal squaramide-based monomers was synthesized to probe their potential to gelate water. The central TREN core with three squaramide units is connected to alkyl chains with a variable number of methylene units (n = 6, 8, 10, or 12) to form the hydrophobic portion of the amphiphile. The hydrophilic domain is composed of tetraethylene glycol monomethyl ether oligomers that are coupled to the hydrophobic domain through a carbamate moiety (**1**-**4**, **Figure 2.1A**). Compounds **1**-**4** were synthesized by reacting tetraethylene glycol monomethyl ether with 1,1-carbonyldiimidazole followed by reaction with an

excess of the carboxybenzyl (Cbz)-protected linear 1, n-alkyldiamine (n = 6, 8, 10, 12) with yields ranging from 48 to 71%. The Cbz protecting group was deprotected by catalytic hydrogenation to reveal an amine moiety, which was further reacted with dibutyl squarate and DIPEA to provide yields of 52-73%. In a final step, the squaramide amphiphile was reacted with TREN to obtain the final tripodal squaramide-based monomers with yields in the range of 42-54% (see Supporting Information). To better understand the role of the squaramide moiety in the self-assembly of the materials (*vide infra*), a control molecule **5** (see Supporting Information) where the three squaramide units in molecule **3** are substituted by three urea moieties, was synthesized with a yield of 56% to substitute.

2.3.2 Supramolecular materials self-assembly

The sol-to-gel transition of the squaramide-based monomers **1**-**4** in aqueous solution were tested by the gel inversion method. Monomers **1**-**4** were all poorly soluble in deionized water, even with heating. Their sonication at room temperature in an ultrasonic bath resulted in their initial dissolution with transparent hydrogels being formed for **2** and **3** from the library (**Figure 2.1B**). Monomer **3** formed gels immediately after sonication when above its critical gelation concentration (CGC) of 1.3-1.9 mM; however, **2** required a significantly higher concentration of the monomer (4.0-4.6 mM) and a longer time for gelation to occur (**Figures S2.1** and **S2.2**). Conversely, **1** formed clear solutions, eventually precipitating at concentrations above 4.2 mM, whereas **4** with the longest alkyl chain (n = 12) was insoluble in water even after a longer sonication period of 1 h. When the squaramide moieties of **3** were replaced with ureas (**5**), clear solutions instead of hydrogels were obtained at a concentration of 3.1 mM. Further increasing the concentration of **5** (5.0 mM) resulted in its precipitation, pointing out the importance of the squaramide motif for gelation of the tripodal monomer in water.

The mechanical properties of hydrogels **2** and **3** were measured by oscillatory rheology in deionized water at 25 °C and also in phosphate buffered saline (PBS) at 37 °C (**Figure 2.2**, **Figures S2.3** and **S2.4**). The linear viscoelastic regime (LVE) was first determined by an amplitude experiment. For a hydrogel composed of **3** in deionized water at 25 °C or in PBS at 37 °C, the storage (G') and loss (G'') moduli remained constant until 3% strain at a fixed frequency of 1.0 Hz, whereas for a hydrogel composed of **2**, both moduli remained constant until the application of 10% strain. In frequency sweep experiments of hydrogels **2** and **3**,

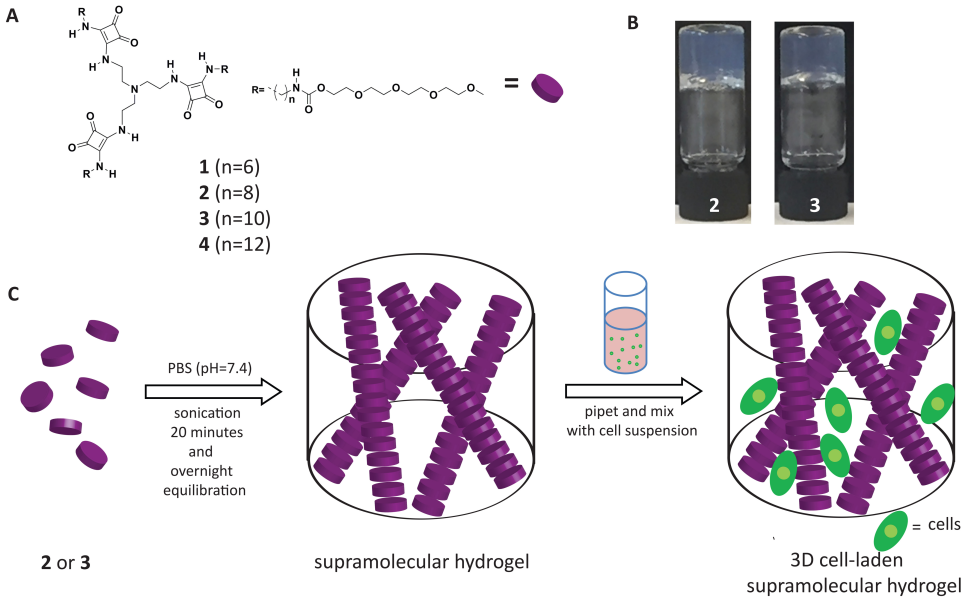

Figure 2.1 (A) Tripodal squaramide-based monomers **1-4** with varied alkyl chain lengths (n = 6, 8, 10, 12). (B) Gel inversion test of squaramide-based materials above the CGC: **2** (5.6 mM) and **3** (3.1 mM) in deionized water. (C) Supramolecular hydrogel preparation and 3D cell seeding strategy.

G' was found to be greater than G'' by nearly an order of magnitude and frequency independent over the measured range from 0.01 to 2.0 Hz, synonymous with the formation of a viscoelastic material. The hydrogels at 37 °C in PBS (G' = 37 Pa for **2**; G' = 64 Pa for **3**) showed similar storage moduli to those at 25 °C in deionized water (G' = 46 Pa for **2**; G' = 67 Pa for **3**). Moreover, step-strain experiments were performed to examine the potential of supramolecular hydrogels **2** and **3** to self-recover after the application of a large strain. When a large amplitude strain was applied (200% for hydrogel **2** and 100% for hydrogel **3** at a frequency of 1.0 Hz in deionized water at 25 °C or in PBS at 37 °C) for 120 s, the G' value of both hydrogels **2** and **3** decreased and showed an inversion of their moduli (G'' > G'). However, when the large amplitude strain was removed, both hydrogels **2** and **3** quickly recovered back to the gel state (G' > G''). The recovery of the hydrogel materials after the application of a cyclic strain was demonstrated over 2 cycles.

To understand the origin of the rheological properties of **2** and **3**, cryogenic transmission electron (cryo-TEM) microscopy was performed. Imaging of the network at the nanoscale by cryo-TEM revealed fibers greater than a micrometer in length with a width of (5.4 ± 1.0) nm for a hydrogel composed of **2** (5.6 mM, **Figure S2.5**) and (4.2 ± 1.1) nm for **3** (3.1 mM, **Figure 2.2D**). Cryo-

electron tomography was further executed on hydrogel **3**, providing a view into the organization of the 3D fibrillar network. Presumably, the gel properties arise from the entanglements of the self-assembled fibers of the squaramide-based monomers (**Figure 2.2E**). This observation is in contrast to cryo-TEM images taken for solutions of **5** after sonication that show domains of fiber alignment rather than entanglement (**Figure S2.6**).[58] The cryo-TEM images of **3** were further supported by small-angle X-ray scattering experiments (SAXS) in the solution phase, where scattering profiles showed the formation of high-aspect-ratio one-dimensional aggregates. The data were best described with a form factor for flexible cylinders, which yielded a cross-sectional radius (rcs) of 2.6 nm, a cross-sectional mass per unit length (ML) of 2.42 × 10^{-21} g nm^{-1}, and a Kuhn length of 6.6 nm (**Figure 2.2F**). By applying eqs 1 and 2 (Supporting Information) and by estimation of the Ics (**Figure S2.9**), 1 monomer/nm was determined along the fibrillar axes. These results indicate that transitioning from a bola-amphiphilic[42] to a pseudo-C3 symmetric monomer geometry reduces lateral monomer aggregation and increases fiber length and flexibility.

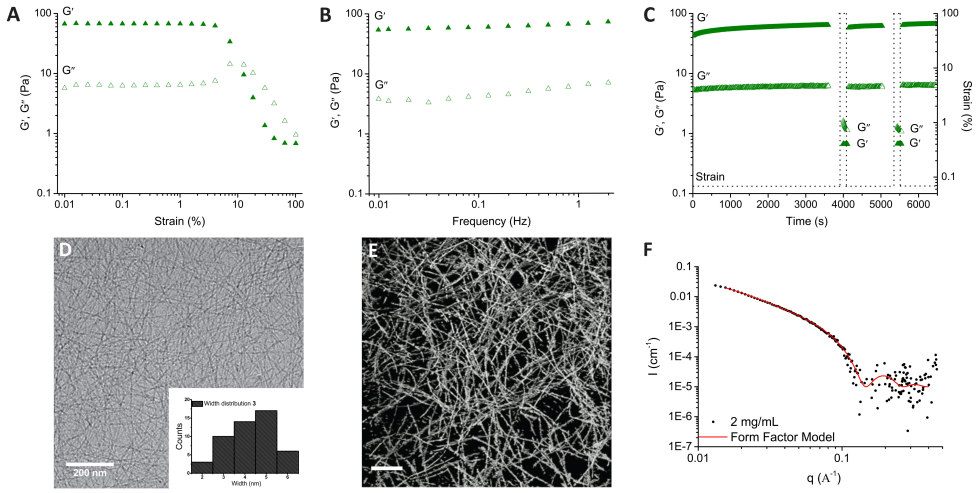

Figure 2.2 Oscillatory rheology measurements of the hydrogel **3** (3.1 mM) in PBS (pH = 7.4) at 37 °C: (A) Amplitude sweep (f = 1 Hz). (B) Frequency sweep (γ = 0.05%). (C) Step strain measurements (f = 1 Hz), the absence of data before the application of high strain is due to the acquisition of a frequency sweep (from 0.01 to 2 Hz, γ = 0.05%). (D) Cryo-TEM image of a hydrogel **3** (3.1 mM). Insert: Histograms of width distribution of the fibres for a sample size of N = 50. (E) Cryo-electron tomography image of a hydrogel of **3** (3.1 mM). Scale bar: *200 nm*. (F) Small-angle X-ray scattering profiles of fibers **3** collected at a concentration of 2 mg mL^{-1}. Black dots represent experimental data; red line represents fit with a form factor for flexible cylinders.

Spectroscopic methods were pursued to gain insight into the effect of the hydrophobic-hydrophilic balance of monomers **1**-**3** on squaramide self-assembly. Monomers **2** and **3** (1.5×10^{-5} M) showed two distinct absorption bands at 255 and 329 nm consistent with simultaneous red- and blue-shifting of the HOMO-LUMO and HOMO-LUMO+1 transition, respectively, upon aggregation (**Figure 2.3A**).[42] Their self-assembly is further supported by cryo-TEM imaging performed on dilute solutions **2** and **3** in water (1.5×10^{-5} M, **Figure S2.7**), which showed the presence of long fibers. Concentration-dependent measurements of **2** and **3** displayed retention of these bands at concentrations as low as 3.75×10^{-6} M for **2** and 1.5×10^{-6} M for **3** (**Figure S2.10**). Conversely, **1** with the shortest alkyl spacer (n = 6) displayed only a single band. The spectrum obtained for **1** in water bears resemblance to the spectra collected for **2** and **3** in hexafluoroisopropanol (HFIP), a low dielectric solvent known to disrupt hydrogen bonds (**Figure S2.11**), and is thus suggestive of a lesser degree of monomer aggregation. Fluorescence measurements using Nile Red as a probe of the hydrophobic environment support the results of the UV-Vis measurements (**Figure 2.3B**). Compound **1** does not affect the fluorescence intensity and maximum wavelength of the Nile Red dye in water, whereas compound **3** showed the greatest increase in fluorescence intensity and blue-shifting (622 nm) of the Nile Red peak (659 nm) relative to **2** (633 nm). Fourier transform infrared (FTIR) spectroscopy on lyophilized samples from gel inversion experiments supported the presence of hydrogen bonding and hydrophobic interactions between the tripodal squaramide-based supramolecular monomers.[42] Samples **1**-**3** displayed two distinct frequencies for the N-H stretch of the carbamate (3317-3315 cm^{-1}) and squaramide units (3167-3164 cm^{-1}). Additionally, the antisymmetric and symmetric C-H stretches were shifted to lower wavenumbers with the increasing length of the alkyl chains (from n = 6 to 10) from 2931 and 2861 cm^{-1} to 2918 and 2850 cm^{-1}, respectively; these are indicative of their close packing within the supramolecular polymer (**Figure 2.3C**, inset).[59,60] All samples showed a small broad band at 1799 cm^{-1} associated with ring breathing of the squaramide unit and one or two C = O stretching modes of the carbamates and squaramides in the amide I region (**Figure 2.3C** and **Table S2.2**). The variable number of bands in the amide I region suggests that more than one packing mode of the various monomers exists in the self-assembled state.

Hence, the squaramide unit can be employed to robustly self-assemble flexible amphiphilic monomers through a combination of hydrophobic and hydrogen bonding interactions into long fibrillar aggregates and eventually gel

phase materials in water. Their mechanical "softness" is attractive for the culture of hiPSCs because of their similar Young's modulus (E~200 Pa using the relationship E~3G for a hydrogel material, where G is the elastic shear modulus[61]) in comparison to embryonic tissues (ranging from tens to several hundreds of Pascals[62-64]). Moreover, the self-recovering character of the squaramide based supramolecular materials opens the door for the gentle encapsulation and release of hiPSCs.

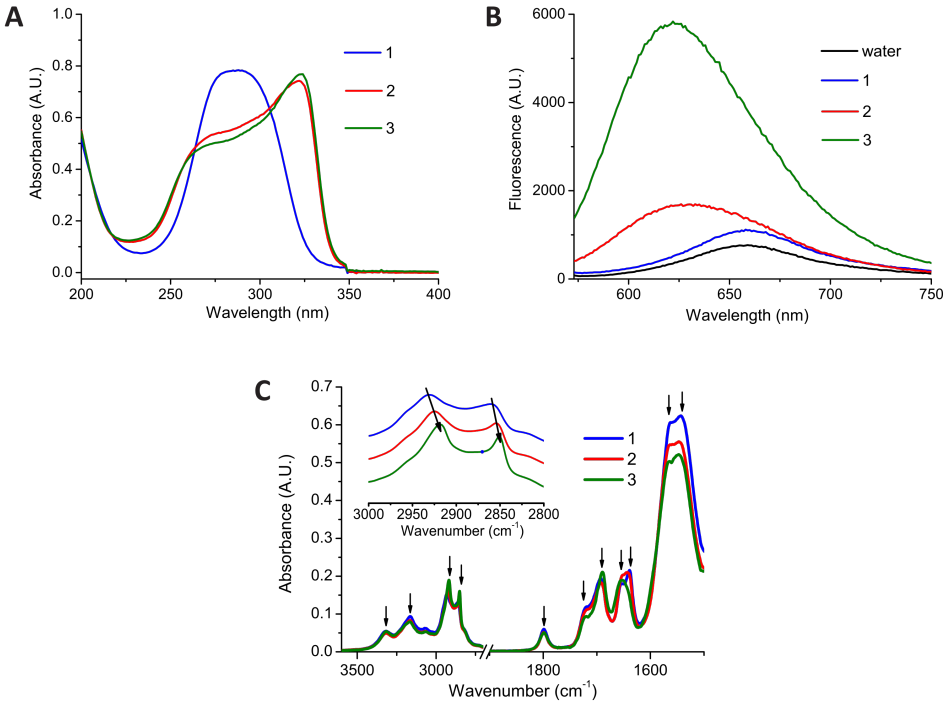

Figure 2.3 (A) UV-Vis spectra of molecules **1-3** in deionized water (1.5×10^{-5} M). (B) Solutions of Nile Red (1.0×10^{-6} M, Ex. 550 nm, Em. 560-750 nm) in deionized water and in the presence of **1-3** (1.5×10^{-5} M). (C) FTIR spectra of samples **1-3** in the solid state (samples lyophilized from deionized water (3.1 mM), arrows highlight peaks considered).

2.3.3 Cell viability and 3D cell culture studies

To apply these tripodal squaramide-based supramolecular polymers in the biomedical area, as either nanoparticles or hydrogel scaffolds, we first evaluated their cytocompatibility with NIH 3T3 cells. The cytotoxicity of monomers **1**-**3** with increasing concentration (1-200 µM) in both water and PBS were evaluated by an MTT cytotoxicity assay (**Figure S2.12**). The cell viability was ~95% for monomers **1**-**3** as the concentration was increased from 1 to 200 µM and applied for 24 and 72

h, similar to the control sample. These results indicate that supramolecular polymers constructed from monomers **1**-**3** in the solution phase are cytocompatible in the range of tested concentrations during the culture period.

As hydrogels, **2** and **3** were further examined for their capacity to encapsulate cells in 3D using their self-recovery character (cell seeding scheme in **Figure 2.1C** and full experimental details in experimental section). For both hydrogels **2** (5.6 mM) and **3** (3.1 mM), 99 and 98% of the cells, respectively, were well-dispersed and viable 2 h after the seeding process as calculated by counting viable cells in fluorescent Z-stack images collected by confocal microscopy (**Figures S2.13** and **S2.14**). Moreover, after 48 h of seeding, 74% of cells seeded in 3D in hydrogel **2** and 77% of cells in hydrogel **3** remained viable, as evidenced by the numerous Calcein AM positive cells and very few propidium iodide stained cells. These results were comparable to other previous hydrogel materials used for 3D cell culture studies, indicating their potential application as synthetic scaffolds *in vitro*.[65-68]

We further examined whether these tripodal squaramide-based materials were suitable for the 3D culture of hiPSC and hiPSC-derived endothelial cells (hiPSC-ECs). First, hiPSC-ECs were encapsulated in hydrogel **3** (with a final concentration of 3.1 mM) using the same technique as for the NIH 3T3 cells. The hiPSC-ECs were well-dispersed throughout the gel, and the majority remained viable after 24 h as observed by the virtual absence of NucGreen Dead positive cells (**Figure S2.15**). Despite being viable, no cell proliferation or cell attachment/spreading of the hiPSC-ECs was observed in the hydrogel, which could be expected based on the lack of adherent cues (e.g., RGD) within the supramolecular matrix. Interestingly, the encapsulation of undifferentiated hiPSCs as single cells in supramolecular hydrogel **3** resulted in the formation of compact spheroids of increasing diameter after 24 h when seeded in 3D. Their formation was followed by time-lapse microscopy over a period of 72 h. Importantly, the hiPSC spheroids remained viable as observed by their morphology and the largely absent staining of dead cells with the NucGreen Dead reagent after 24 and 72 h (**Figure 2.4A**, **B**). The evolution of the hiPSC spheroid diameter after encapsulation of single hiPSCs in hydrogel **3** (3.1 mM) over time (24, 48, and 72 h culture) was observed to trend to larger sizes with longer culture periods (after 72 h, spheroid diameters ranged from 26 to 143 µm from single cells on day 0) and indicates that the supramolecular hydrogels do not interfere with the cell-cell contacts typically

formed by these undifferentiated cells (representative images of hiPSC spheroids in the hydrogel are shown in **Figure 2.4C** and **Figure S2.16**).

A major difficulty in the culture of hiPSCs is developing a facile way to release them when encapsulated in 3D for downstream analysis or passage because enzymatic methods may not be effective.[69] This challenge has prompted the development of materials that enable cell release from a 3D environment in response to a temperature change or UV light.[70,71] Therefore, we examined the potential to gently release the hiPSCs from the squaramide-based supramolecular hydrogel materials by their simple mechanical disruption by pipetting and dilution into a ~50× greater volume of PBS for analysis of pluripotent markers by fluorescence-activated cell sorting (FACS). More specifically, cell surface expression of TRA-1-60 and SSEA-4, pluripotent stem cell markers associated with the undifferentiated state, were analyzed after their dissociation into single cells and compared against hiPSCs cultured in standard maintenance conditions (e.g., vitronectin coated plates in TeSR-E8 medium), as shown comparing histograms of fluorescence intensity of the above-mentioned markers in the gated live cell population (**Figure 2.4D**). The values of mean fluorescence intensity (MFI) for the TRA-1-60 and SSEA-4 markers for hiPSCs cultured on a 2D surface and the hydrogels in 3D were positive during the culture period, with greater values measured for the hydrogels in 3D (**Figure S2.17**). Moreover, the percentage of live hiPSCs cells, as determined by side scatter (SSC-A) and forward scatter (FSC-A) events, were comparable between the 2D and 3D cultures.

Overall, the squaramide-based supramolecular hydrogels proved to be cytocompatible toward any of the cell types tested, including sensitive cells such as hiPSCs and their derivatives. The supramolecular polymer materials permitted spheroid formation from single cells and the hiPSCs retained their pluripotent state during the culture period and upon release. However, to better understand the full potential of these squaramide-based supramolecular materials for future applications such as expansion or directed differentiation, the examination of longer culture periods within the materials alongside the incorporation of bioactive cues will be necessary.

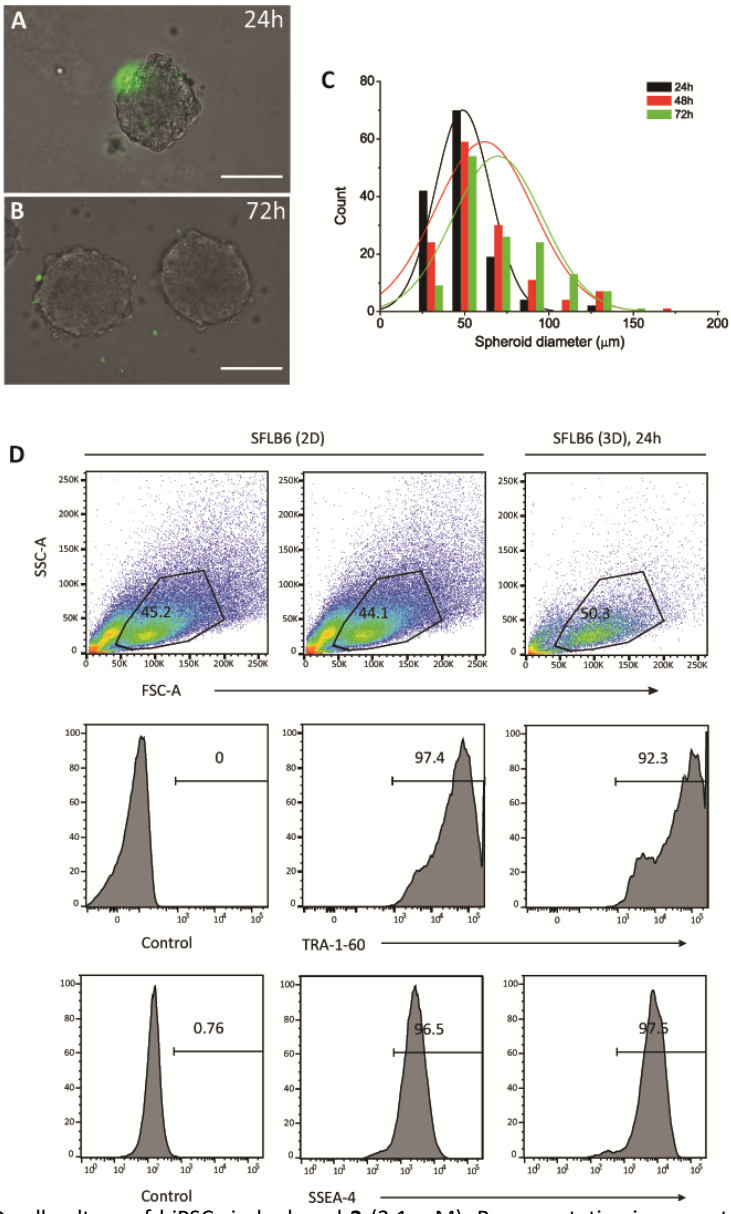

Figure 2.4 3D cell culture of hiPSCs in hydrogel **3** (3.1 mM): Representative images at ~24 (A) and ~72 h (B). Dead cells were detected using the NucGreen® Dead reagent. Scale bar: *100 µm*. (C) Distribution of spheroid diameters in a hydrogel of **3** (3.1 mM) after 24 h, 48 h and 72 h; approximately 135 spheroids per day were measured. (D) FACS analysis of single cells of hiPSCs cultured under standard conditions in 2D (*left control*, *middle with TRA-1-60 and SSEA-4 antibodies*) on a vitronectin surface or after retrieval from hydrogel **3** (3.1 mM) after 24 h of culture (*right with TRA-1-60 and SSEA-4 antibodies*). Upper panel: side scatter (SSC-A) and forward scatter (FSC-A) showing live cell population (Black circles are the gated live cells); Lower panel: expression level of TRA-1-60 and SSEA-4 pluripotent stem cell markers of the gated live cells.

2.4 Conclusions

A novel family of minimalistic tripodal squaramide-based monomers containing a flexible TREN core with varied hydrophobic (n = 6, 8, 10, 12) and hydrophilic domains were successfully synthesized and characterized. The tripodal geometry was selected to increase number of non-covalent interactions, reduce free monomer aggregation, and increase the directional fiber formation. Self-recovering hydrogels were formed under physiological conditions at 37 °C when alkyl chain lengths of 8 and 10 carbons were used. Additionally, cryo-TEM and SAXS measurements of these hydrogels showed the formation of a network composed of entangled fibrils that were a few nanometers in width and micrometers in length. Spectroscopic measurements provided insight into the self-assembly properties of the squaramide-based supramolecular polymers at the molecular scale, indicating that hydrogen bonding and hydrophobic interactions facilitate their self-assembly. For 3D cell culture, a cytocompatible response was observed for a range of cell types, including several considered sensitive such as hiPSCs and their differentiated derivatives. Moreover, the hiPSCs produced spheroids from single cells within the supramolecular hydrogels, suggesting that these materials do not interfere with their formation through cell-cell contact. Finally, the hiPSCs retain their pluripotent stem cell phenotype upon gentle isolation of the spheroids by simple dilution from the squaramide-based supramolecular material and further dissociation into single cells for FACS analysis. The simplicity of the seeding and release approach in 3D combined with the cytocompatibility of these squaramide-based materials opens the door to further explore their use for applications in 3D cell culture and delivery, namely with hiPSCs and cells that are derived from them.

2.5 References

(1) Amabilino, D. B.; Smith, D. K.; Steed, J. W. *Chem. Soc. Rev.* **2017**, *46* (9), 2404-2420.

(2) Krieg, E.; Bastings, M. M.; Besenius, P.; Rybtchinski, B. *Chem. Rev.* **2016**, *116* (4), 2414-2477.

(3) Aida, T.; Meijer, E.; Stupp, S. *Science* **2012**, *335* (6070), 813-817.

(4) Webber, M. J.; Appel, E. A.; Meijer, E.; Langer, R. *Nat. Mater.* **2016**, *15* (1), 13-26.

(5) Rudra, J. S.; Tian, Y. F.; Jung, J. P.; Collier, J. H. *Proc. Natl. Acad. Sci. U. S. A.* **2010**, *107* (2), 622-627.

(6) Stephanopoulos, N.; Freeman, R.; North, H. A.; Sur, S.; Jeong, S. J.; Tantakitti, F.; Kessler, J. A.; Stupp, S. I. *Nano Lett.* **2015**, *15* (1), 603-609.

(7) Hudalla, G. A.; Sun, T.; Gasiorowski, J. Z.; Han, H.; Tian, Y. F. Chong, A. S.; Collier, J. H. *Nat. Mater.* **2014**, *13* (8), 829-836.

(8) Rodell, C. B.; Dusaj, N. N.; Highley, C. B.; Burdick, J. A. *Adv. Mater.* **2016**, *28* (38), 8419-8424.

(9) Bastings, M.; Koudstaal, S.; Kieltyka, R. E.; Nakano, Y.; Pape, A.; Feyen, D. A.; Van Slochteren, F. J.; Doevendans, P. A.; Sluijter, J. P.; Meijer, E.; Chamuleau, S. A. J.; Dankers, P. Y. W. *Adv. Healthcare Mater.* **2014**, *3* (1), 70-78.

(10) Li, Y.; Khuu, N.; Gevorkian, A.; Sarjinsky, S.; Therien-Aubin, H.; Wang, Y.; Cho, S.; Kumacheva, E. *Angew. Chem. Int. Ed.* **2017**, *129* (22), 6179-6183.

(11) Sinthuvanich, C.; Nagy-Smith, K. J.; Walsh, S. T.; Schneider, J. P. *Macromolecules* **2017**, *50* (15), 5643-5651.

(12) Johnson, E. K.; Adams, D. J.; Cameron, P. J. *J. Mater. Chem.* **2011**, *21* (7), 2024-2027.

(13) Wang, Y.; Cheetham, A. G.; Angacian, G.; Su, H.; Xie, L.; Cui, H. A*dv. Drug Delivery Rev.* **2017**, *110*, 112-126.

(14) Ikonen, L.; Kerkelä, E.; Metselaar, G.; Stuart, M. C.; De Jong, M. R.; Aalto-Setälä, K. *Bio. Med. Res. Int.* **2013**, *2013*, 1-12.

(15) Takahashi, K.; Tanabe, K.; Ohnuki, M.; Narita, M.; Ichisaka, T. Tomoda, K.; Yamanaka, S. *Cell* **2007**, *131* (5), 861-872.

(16) Yu, J.; Vodyanik, M. A.; Smuga-Otto, K.; Antosiewicz-Bourget, J.; Frane, J. L.; Tian, S.; Nie, J.; Jonsdottir, G. A.; Ruotti, V.; Stewart, R.; Slukvin, I. I.; Thomson, J. A. *Science* **2007**, *318* (5858), 1917-1920.

(17) Higuchi, A.; Ling, Q. D.; Chang, Y.; Hsu, S. T.; Umezawa, *Chem. Rev.* **2013**, *113* (5), 3297-3328.

(18) Higuchi, A.; Ling, Q. D.; Kumar, S. S.; Munusamy, M.; Alarfajj, A. A.; Umezawa, A.; Wu, G. J. *Prog. Polym. Sci.* **2014**, *39* (7), 1348-1374.

(19) Higuchi, A.; Ling, Q. D.; Ko, Y. A.; Chang, Y.; Umezawa, *Chem. Rev.* **2011**, *111* (5), 3021-3035.

(20) Peng, I. C.; Yeh, C. C.; Lu, Y. T.; Muduli, S.; Ling, Q. D.; Alarfaj A. A.; Munusamy, M. A.; Kumar, S. S.; Murugan, K.; Lee, H. C. Chang, Y.; Higuchi, A. *Biomaterials* **2016**, *76*, 76-86.

(21) Rosales, A. M.; Anseth, K. S. *Nat. Rev. Mater.* **2016**, *1*, 15012.
(22) Cosson, S.; Otte, E. A.; Hezaveh, H.; Cooper-White, J. J. *Stem Cells Transl. Med.* **2015**, *4* (2), 156-164.
(23) Rehm, T.; Schmuck, C. *Chem. Commun.* **2008**, *7*, 801-813.
(24) Rao, K. V.; George, S. J. *Chem. Eur. J.* **2012**, *18* (45), 14286-14291.
(25) Krieg, E.; Weissman, H.; Shimoni, E.; Bar On, A.; Rybtchinski, B. *J. Am. Chem. Soc.* **2014**, *136* (26), 9443-9452.
(26) Yu, Z.; Tantakitti, F.; Yu, T.; Palmer, L. C.; Schatz, G. C.; Stupp, S. I. *Science* **2016**, *351* (6272), 497-502.
(27) Appel, R.; Fuchs, J.; Tyrrell, S. M.; Korevaar, P. A.; Stuart, M. C.; Voets, I. K.; Schönhoff, M.; Besenius, P. *Chem. Eur. J.* **2015**, *21* (52), 19257-19264.
(28) Rao, K. V.; Jayaramulu, K.; Maji, T. K.; George, S. J. *Angew. Chem. Int. Ed.* **2010**, *122* (25), 4314-4318.
(29) Kluge, D.; Singer, J. C.; Neubauer, J. W.; Abraham, F.; Schmidt, H. W.; Fery, A. *Small* **2012**, *8* (16), 2563-2570.
(30) Wilson, A. J. *Soft Matter* **2007**, *3* (4), 409-425.
(31) Leenders, C. M.; Albertazzi, L.; Mes, T.; Koenigs, M. M.; Palmans, A. R.; Meijer, E. *Chem. Commun.* **2013**, *49* (19), 1963-1965.
(32) Mes, T.; Cantekin, S.; Balkenende, D. W.; Frissen, M. M.; Gillissen, M. A.; De Waal, B. F.; Voets, I. K.; Meijer, E.; Palmans, A. R. *Chem. Eur. J.* **2013**, *19* (26), 8642-8649.
(33) Chebotareva, N.; Bomans, P. H.; Frederik, P. M.; Sommerdijk, N. A.; Sijbesma, R. P. *Chem. Commun.* **2005**, *39*, 4967-4969.
(34) Shimizu, L. S.; Hughes, A. D.; Smith, M. D.; Davis, M. J.; Zhang, B. P.; zur Loye, H.-C.; Shimizu, K. D. *J. Am. Chem. Soc.* **2003**, *125* (49), 14972-14973.
(35) Li, A. F.; Wang, J. H.; Wang, F.; Jiang, Y. B. *Chem. Soc. Rev.* **2010**, *39* (10), 3729-3745.
(36) Dingels, C.; Wurm, F.; Wagner, M.; Klok, H. A.; Frey, H. *Chem. Eur. J.* **2012**, *18* (52), 16828-16835.
(37) Olmo, F.; Rotger, C.; Ramírez-Macías, I.; Martínez, L.; Marín, C.; Carreras, L.; Urbanová, K.; Vega, M.; Chaves-Lemaur, G.; Sampedro, A.; Rosales, M. J. *J. Med. Chem.* **2014**, *57* (3), 987-999.
(38) Malerich, J. P.; Hagihara, K.; Rawal, V. H. *J. Am. Chem. Soc.* **2008**, *130* (44), 14416-14417.
(39) Busschaert, N.; Kirby, I. L.; Young, S.; Coles, S. J.; Horton, P. N.; Light, M. E.; Gale, P. A. *Angew. Chem. Int. Ed.* **2012**, *51* (18), 4426-4430.
(40) Schiller, J.; Alegre-Requena, J. V.; Marqués-López, E.; Herrera, R. P.; Casanovas, J.; Alemán, C.; Díaz, D. D. *Soft Matter* **2016**, *12* (19), 4361-4374.
(41) Wu, D.; Jiang, R.; Luo, L.; He, Z.; You, J. *Inorg. Chem. Front.* **2016**, *3* (12), 1597-1603.
(42) Saez Talens, V.; Englebienne, P.; Trinh, T. T.; Noteborn, W. E.; Voets, I. K.; Kieltyka, R. E. *Angew. Chem. Int. Ed.* **2015**, *127* (36), 10648-10652.
(43) López, C.; Ximenis, M.; Orvay, F.; Rotger, C.; Costa, A. *Chem. Eur. J.* **2017**, *23* (31),

7590-7594.
(44) Noteborn, W. E.; Saez Talens, V.; Kieltyka, R. E. *Chem. Bio. Chem.* **2017**, *18* (20), 1995-1999.
(45) Storer, R. I.; Aciro, C.; Jones, L. H. *Chem. Soc. Rev.* **2011**, *40* (5), 2330-2346.
(46) Alemán, J.; Parra, A.; Jiang, H.; Jørgensen, K. A. *Chem. Eur. J.* **2011**, *17* (25), 6890-6899.
(47) Cantekin, S.; de Greef, T. F.; Palmans, A. R. *Chem. Soc. Rev.* **2012**, *41* (18), 6125-6137.
(48) van Bommel, K. J.; van der Pol, C.; Muizebelt, I.; Friggeri, A.; Heeres, A.; Meetsma, A.; Feringa, B. L.; van Esch, J. *Angew. Chem. Int. Ed.* **2004**, *43* (13), 1663-1667.
(49) Ageitos, J. M.; Baker, P. J.; Sugahara, M.; Numata, K. *Biomacromolecules* **2013**, *14* (10), 3635-3642.
(50) Stanley, C. E.; Clarke, N.; Anderson, K. M.; Elder, J. A.; Lenthall, J. T.; Steed, J. W. *Chem. Commun.* **2006**, *30*, 3199-3201.
(51) Hiscock, J. R.; Piana, F.; Sambrook, M. R.; Wells, N. J.; Clark, A. J.; Vincent, J. C.; Busschaert, N.; Brown, R. C.; Gale, P. A. *Chem. Commun.* **2013**, *49* (80), 9119-9121.
(52) Mukhopadhyay, S.; Maitra, U.; Krishnamoorthy, G.; Schmidt, J.; Talmon, Y. *J. Am. Chem. Soc.* **2004**, *126* (48), 15905-15914.
(53) de Loos, M.; Ligtenbarg, A. G.; van Esch, J.; Kooijman, H.; Spek, A. L.; Hage, R.; Kellogg, R. M.; Feringa, B. L. *Eur. J. Org. Chem.* **2000**, *22*, 3675-3678.
(54) Kremer, J. R.; Mastronarde, D. N.; McIntosh, J. R. *J. Struct. Biol.* **1996**, *116* (1), 71-76.
(55) Pettersen, E. F.; Goddard, T. D.; Huang, C. C.; Couch, G. S.; Greenblatt, D. M.; Meng, E. C.; Ferrin, T. E. J. *Comput. Chem.* **2004**, *25* (13), 1605-1612.
(56) Zhang, M.; D'Aniello, C.; Verkerk, A. O.; Wrobel, E.; Frank, S.; Ward-vanOostwaard, D.; Piccini, I.; Freund, C.; Rao, J.; Seebohm, G. *Proc. Natl. Acad. Sci. U. S. A.* **2014**, *111* (50), E5383-E5392.
(57) Orlova, V. V.; Van Den Hil, F. E.; Petrus-Reurer, S.; Drabsch, Y.; Ten Dijke, P.; Mummery, C. L. *Nat. Protoc.* **2014**, *9* (6), 1514-1531.
(58) Zhang, X.; Chu, X.; Wang, L.; Wang, H.; Liang, G.; Zhang, J.; Long, J.; Yang, Z. *Angew. Chem. Int. Ed.* **2012**, *124*, 4464-4468.
(59) Nebot, V. J.; Armengol, J.; Smets, J.; Prieto, S. F.; Escuder, B.; Miravet, J. F. *Chem. Eur. J.* **2012**, *18* (13), 4063-4072.
(60) Yang, M.; Zhang, Z.; Yuan, F.; Wang, W.; Hess, S.; Lienkamp, K.; Lieberwirth, I.; Wegner, G. *Chem. Eur. J.* **2008**, *14* (11), 3330-3337.
(61) Caliari, S. R.; Burdick, J. A. *Nat. Methods* **2016**, *13* (5), 405-414.
(62) Caiazzo, M.; Okawa, Y.; Ranga, A.; Piersigilli, A.; Tabata, Y.; Lutolf, M. P. *Nat. Mater.* **2016**, *15* (3), 344-352.
(63) Kinney, M. A.; Saeed, R.; McDevitt, T. C. *Sci. Rep.* **2015**, *4*, 4290.
(64) Kolahi, K. S.; Donjacour, A.; Liu, X.; Lin, W.; Simbulan, R. K.; Bloise, E.; Maltepe, E.; Rinaudo, P. *PLoS One* **2012**, *7* (7), e41717.
(65) McKinnon, D. D.; Domaille, D. W.; Cha, J. N.; Anseth, K. S. *Adv. Mater.* **2014**, *26* (6),

865-872.
(66) Costa, A. M.; Mano, J. F. *Chem. Commun.* **2015**, *51* (86), 15673-15676.
(67) Hodgson, S. M.; McNelles, S. A.; Abdullahu, L.; Marozas, I. A.; Anseth, K. S.; Adronov, A. *Biomacromolecules* **2017**, *18* (12), 4054-4059.
(68) Brown, T. E.; Silver, J. S.; Worrell, B. T.; Marozas, I. A.; Yavitt, F. M.; Gunay, K. A.; Bowman, C. N.; Anseth, K. S. *J. Am. Chem. Soc.* **2018**, *140* (37), 11585-11588.
(69) Caliari, S. R.; Burdick, J. A. *Nat. Methods* **2016**, *13* (5), 405-414.
(70) Shin, D. S.; You, J.; Rahimian, A.; Vu, T.; Siltanen, C.; Ehsanipour, A.; Stybayeva, G.; Sutcliffe, J.; Revzin, A. *Angew. Chem. Int. Ed.* **2014**, *53* (31), 8221-8224.
(71) Lei, Y.; Schaffer, D. V. *Proc. Natl. Acad. Sci. U. S. A.* **2013**, *110* (52), E5039-E5048.

2.6 Supporting Information

2.6.1 Materials and instruments

All chemicals and reagents for the synthesis of the tripodal squaramide-based monomers were obtained from commercial suppliers and used without further purification. Deuterated dimethyl sulfoxide, methanol, and chloroform were purchased from Euriso-top. Dulbecco's modified Eagle medium (DMEM) was obtained from Gibco, Life Technologies. Eight-well Lab-Tek slides and the NucGreen Dead reagent were purchased from Thermo Fisher Scientific. Propidium Iodide (PI), calcein AM (AM = acetoxymethyl), and 3-[4,5-dimethyl-2-thiazolyl]-2,5-diphenyl-2H-tetrazolium bromide (MTT) were purchased from Sigma-Aldrich. TeSR-E8 cell culture medium was purchased from STEMCELL Technologies, and TrypLE Select Enzyme together with RevitaCell (1:100) were from Invitrogen. TRA-1-60 (Podocalyxin) and SSEA-4-VioBlue fluorescently labeled monoclonal antibodies were from Miltenyi Biotec, and EGM-2 medium was purchased from PromoCell. Water was deionized prior to use. Purification of the tripodal squaramide-based monomers **1**-**4** was carried out on a Grace Reveleris X1 flash chromatography system equipped with a C18 column, and subsequently by RP-HPLC on a Vydac C18 reversed phase column with UV detection. The tripodal urea-based monomer **5** was purified using an Agilent 1200 HPLC system equipped with a C18 column using mass detection on an Agilent Technologies Q6130. ^{1}H-NMR and ^{13}C-NMR spectra were recorded on a Bruker DMX-400 (400 MHz) operating at 400 MHz for ^{1}H-NMR and 100 MHz for ^{13}C-NMR at 298 K. LC-MS data were collected on a Finnigan Surveyor HPLC system equipped with a Gemini C18 column (50 × 4.60 mm, UV detection from 200 to 600 nm) and coupled to a Finnigan LCQ Advantage Max mass spectrometer with ESI. The gradient for the mobile phase was 10-90% of CH_3CN-H_2O (0.1% TFA) over 13.5 min. Matrix-assisted laser desorption ionization-time-of-flight mass spectra (MALDI-TOF-MS) were recorded on a Bruker microflex LRF mass spectrometer in linear positive-ion mode using α-cyano-4-hydroxycinnamic acid as a matrix on a ground steel target plate. Oscillatory rheology experiments were performed on a Discovery hybrid rheometer DHR-2 (TA Instruments) using cone-plate geometry (40 mm, 1.995°) at (25 ± 0.2) °C or (37 ± 0.2) °C with a Peltier-based temperature control and a solvent trap. Cryo-TEM samples were prepared by applying to a freshly glow-discharged 300 mesh copper grid with a lacey-carbon support film (Supplier-Electron Microscopy Sciences). Excess liquid was blotted away for 2 s (95%

humidity, 21 °C, Whatman No. 4 filter paper) and plunge-frozen in liquid ethane at -183 °C using a Leica EM GP (Leica Microsystems) before imaging. Cryo-TEM images of the vitrified samples were acquired with a Tecnai F20 microscope (FEI) equipped with a field emission gun operating at 200 keV using a Gatan UltraScan charge-coupled device (CCD) camera with a defocus between -6 and -9 µm. Tomographic tilt series were acquired at a magnification of ×29k using a continuous tilt scheme from -51° to +51° in 3° increments, focusing to -8 µm every third image using a low-dose routine. The tomogram was processed using IMOD,[1] aligned using patch tracking methods and reconstructed using 5 iterations of simultaneous iterative reconstruction technique (SIRT). For visualization, the tomogram was low pass filtered to 5 nm and binned 2× for a final pixel size of 1.6 nm. Disconnected particles larger than 200 voxels were removed using UCSF Chimera.[2] Small angle X-ray scattering measurements were performed on a SAXSLAB GANESHA 300 XL SAXS system equipped with a GeniX 3D Cu ultralow divergence microfocus sealed tube source producing X-rays with a wavelength of λ = 1.54 Å at a flux of 1 × 108 ph/s and a Pilatus 300 K silicon pixel detector with 487 × 619 pixels of 172 × 172 µm in size placed at two sample-to-detector distances of 713 and 1513 mm, respectively, to access a q-range of 0.009 ≤ q ≤0.456 Å−1, where $q = 4\pi/\lambda(\sin \theta/2)$. The calibration of the beam center and q-range was achieved by using silver behenate. The SAXS patterns were brought to an absolute intensity scale using the calibrated detector response function, known sample-to-detector distance, measured incident, and transmitted beam intensities and were azimuthally averaged to obtain one-dimensional SAXS profiles. The scattering curves of the self-assembled fibers were obtained by subtraction of the scattering contribution of the solvent and quartz cell using SAXS utilities in the software package (http://www.sztucki.de/SAXSutilities/). The resulting SAXS profiles were analyzed using the software package SASview (http://www.sasview.org/). UV-Vis spectra were recorded on a Cary 300 spectrophotometer (Agilent) using a quartz cuvette with a path length of 1 cm. Fluorescence spectra were acquired on a TECAN Infinite M1000 PRO fluorescent plate reader. Fourier Transform Infrared (FTIR) Spectroscopy were recorded on a PerkinElmer Spectrum Two UATR FT-IR spectrometer with a resolution of 4 cm^{-1}. Hydrogel encapsulated cells in 3D were imaged on a Zeiss LSM 710 confocal laser scanning microscope equipped with a Zeiss 5× objective. Time-lapse imaging was performed using the EVOS FL AUTO2 system. Fluorescence-activated cell sorting (FACS) was performed to quantify the undifferentiated state of hiPSCs.

2.6.2 Synthetic routes and procedures

Synthetic routes of monomers 1-5

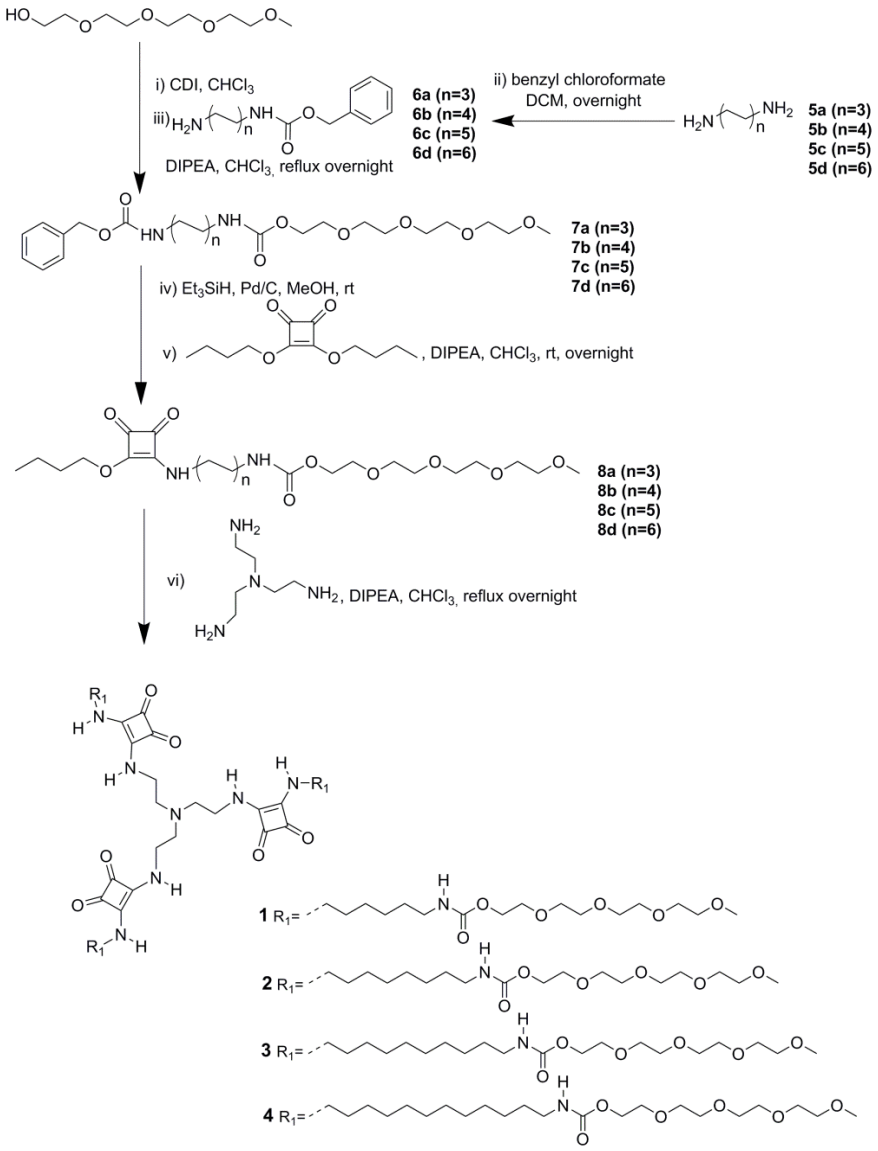

Scheme S2.1 Synthetic route of monomers **1**-**4**.

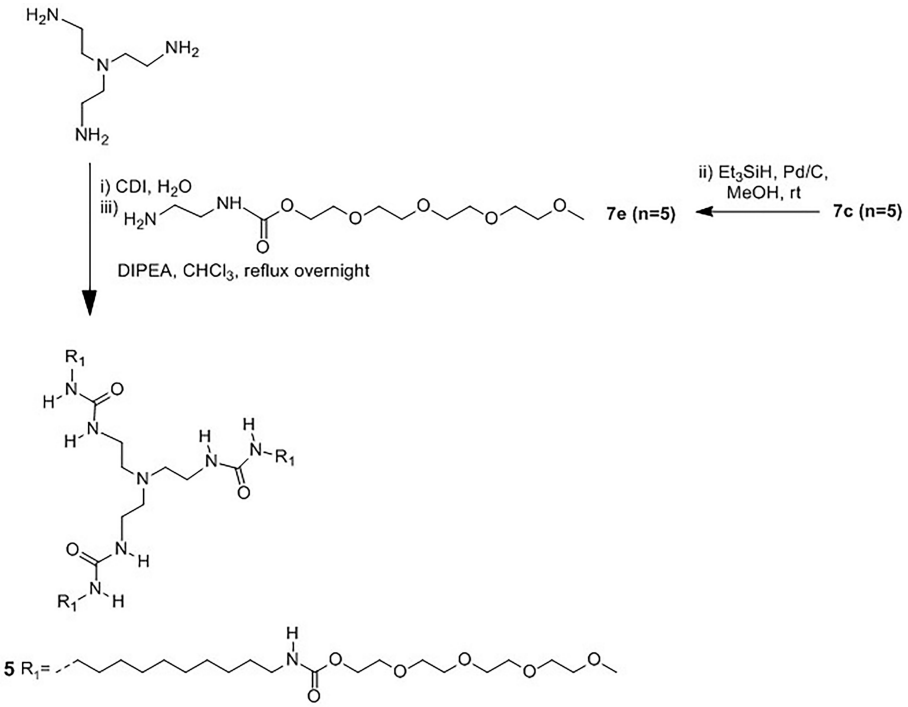

Scheme S2.2 Synthetic route of monomer **5**.

Synthesis of compounds 6a-d

To a solution of benzyl chloroformate (**a**: 2.94 g, 17.23 mmol; **b**: 1.89 g, 11.08 mmol; **c**: 1.98 g, 11.61 mmol; **d**: 1.11 g, 6.51 mmol) in CH_2Cl_2 (100 mL) a stirred solution of the corresponding 1, n-alkyldiamine (**5a** (n = 6): 10.00 g, 86.14 mmol; **5b** (n = 8): 8.03 g, 55.66 mmol; **5c** (n = 10): 10.00 g, 58.05 mmol; **5d** (n = 12): 6.49 g, 32.39 mmol) in CH_2Cl_2 (100 mL) was added dropwise over 2 hours at 0°C. The reaction mixture was allowed to stir overnight at room temperature. The solution was then concentrated by rotary evaporation and EtOAc was added. The mixture washed 3x with water and the aqueous layers were discarded. The organic layer was dried over $MgSO_4$ and the solvent was removed under vacuum to obtain a white solid (**6a**) without further purification. For **6b**-**d**, when 1 M HCl was added, a white precipitate formed in the organic layer. The solid was collected by filtration, washed with EtOAc and used without further purification.

Compound 6a

Yield: 2.67 g, 62%. ^{1}H-NMR (CD_3OD, 400 MHz): 7.34-7.28 (m, 5H), 5.06 (s, 2H), 3.12-3.09 (m, 2H), 2.64-2.60 (m, 2H), 1.51-1.43 (m, 4H), 1.35-1.32 (m, 4H). ^{13}C-

NMR (CD_3OD, 100 MHz): 158.85, 138.44, 129.21, 128.90, 128.71, 67.24, 42.28, 41.66, 33.33, 30.81, 27.56, 27.38. MALDI-TOF-MS: m/z calc: 250.17, found: 250.47 $[M+H]^+$.

Compound 6b

Yield: 2.31 g, 75%. ^{1}H-NMR (CD_3OD, 400 MHz): 7.34-7.27 (m, 5H), 5.06 (s, 2H), 3.12-3.07 (m, 2H), 2.94-2.89 (m, 2H), 1.69-1.63 (m, 2H), 1.53-1.46 (m, 2H), 1.41-1.31 (m, 8H). ^{13}C-NMR (CD_3OD, 100 MHz): 158.49, 138.07, 129.13, 128.60, 128.48, 66.82, 41.28, 40.32, 30.41, 29.64, 28.09, 27.20, 26.92, 26.90. MALDI-TOF-MS: m/z calc: 278.20, found: 278.59 $[M+H]^+$.

Compound 6c

Yield: 2.77 g, 78%. ^{1}H-NMR (CD_3OD, 400 MHz): 7.34-7.27 (m, 5H), 5.06 (s, 2H), 3.11-3.08 (m, 2H), 2.93-2.89 (m, 2H), 1.67-1.62 (m, 2H), 1.50-1.46 (m, 2H), 1.40-1.32 (m, 12H). ^{13}C-NMR (CD_3OD, 100 MHz): 158.47, 138.07, 129.11, 128.56, 128.39, 66.81, 41.35, 40.34, 30.46, 30.08, 29.96, 29.90, 29.74, 28.13, 27.35, 27.00. MALDI-TOF-MS: m/z calc: 306.23, found: 306.65 $[M+H]^+$.

Compound 6d

Yield: 1.39 g, 64%. ^{1}H-NMR (CD_3OD, 400 MHz): 7.34-7.27 (m, 5H), 5.06 (s, 2H), 3.12-3.07 (m, 2H), 2.92-2.89 (m, 2H), 1.67-1.61 (m, 2H), 1.49-1.46 (m, 2H), 1.41-1.30 (m, 16H). ^{13}C-NMR (CD_3OD, 100 MHz): 158.90, 138.50, 129.43, 128.75, 128.69, 67.24, 41.79, 40.77, 30.91, 30.66, 30.64, 30.60, 30.48, 30.39, 30.22, 28.58, 27.82, 27.45. MALDI-TOF-MS: m/z calc: 334.26, found: 334.67 $[M+H]^+$.

Synthesis of compounds 7a-d

Tetraethyleneglycol monomethyl ether (**a**: 1.03 g, 4.95 mmol; **b**: 1.30 g, 6.24 mmol; **c**: 1.50 g, 7.20 mmol; **d**: 1.30 g, 6.24 mmol) was first activated with 1,1'-carbonyldiimidazole (**a**: 0.88 g, 5.44 mmol; **b**: 1.11 g, 6.85 mmol; **c**: 1.28 g, 7.92 mmol; **d**: 1.11 g, 6.87 mmol) for 1 hour at room temperature. Subsequently, **6a-d** (**6a**: 1.49 g, 5.94 mmol; **6b**: 2.08 g, 7.49 mmol; **6c**: 2.65 g, 8.64 mmol; **6d**: 2.50 g, 7.49 mmol), DIPEA (**a**: 1.7 mL, 9.90 mmol; **b**: 2.2 mL, 12.48 mmol; **c**: 2.5 mL, 14.41 mmol; **d**: 2.2 mL, 12.48 mmol) and $CHCl_3$ (15 mL) were added to the reaction mixture and refluxed overnight. Once the reaction was finished, CH_2Cl_2 (15 mL) was added and washed with H_2O (30 mL). The combined aqueous fractions were

then back extracted 3x with CH_2Cl_2 (3 x 30 mL). The combined organic fractions were dried with $MgSO_4$, prior to removal of the solvent in vacuo. The crude product was purified by silica column chromatography using a CH_2Cl_2/EtOAc gradient (20-50 vol% EtOAc). The product was evaporated to dryness by rotary evaporation to obtain a white solid 7a-d and placed in a vacuum oven overnight.

Compound 7a

Yield: 1.46 g, 61%. ^{1}H-NMR ($CDCl_3$, 400 MHz): 7.29-7.24 (m, 5H), 5.20 (br s, 1H), 5.11 (br s, 1H), 5.03 (s, 2H), 4.15-4.13 (m, 2H), 3.76-3.58 (m, 12H), 3.50-3.48 (m, 2H), 3.32 (s, 3H), 3.13-3.05 (m, 4H), 1.45-1.38 (m, 4H), 1.27-1.21 (m, 4H). ^{13}C-NMR ($CDCl_3$, 100 MHz): 156.23, 136.42, 128.35, 128.01, 127.84, 71.69, 70.37, 70.31, 70.27, 69.43, 66.34, 63.60, 58.79, 40.65, 40.57, 29.62, 26.02. LC-MS: t = 6.66 min, m/z: 485.27 $[M+H]^+$. MALDI-TOF-MS: m/z calc: 484.28, found: 506.81 $[M+Na]^+$.

Compound 7b

Yield: 2.26 g, 71%. ^{1}H-NMR ($CDCl_3$, 400 MHz): 7.33-7.25 (m, 5H), 5.06 (s, 2H), 4.98 (br s, 1H), 4.89 (br s, 1H), 4.18-4.16 (m, 2H), 3.65-3.60 (m, 12H), 3.53-3.51 (m, 2H), 3.34 (s, 3H), 3.17-3.08 (m, 4H), 1.47-1.42 (m, 4H), 1.25 (s, 8H). ^{13}C-NMR ($CDCl_3$, 100 MHz): 156.17, 136.38, 128.52, 128.17, 127.98, 71.59, 70.27, 70.21, 70.17, 69.35, 66.24, 63.46, 59.03, 40.76, 40.67, 29.59, 28.83, 26.32. LC-MS: t = 7.37 min, 513.33 m/z $[M+H]^+$. MALDI-TOF-MS: m/z calc: 512.31, found: 534.88 $[M+Na]^+$.

Compound 7c

Yield: 2.45 g, 63%. ^{1}H-NMR ($CDCl_3$, 400 MHz): 7.35-7.29 (m, 5H), 5.08 (s, 2H), 4.83 (br s, 1H), 4.77 (br s, 1H), 4.21-4.19 (m, 2H), 3.68-3.62 (m, 12H), 3.55-3.53 (m, 2H), 3.37 (s, 3H), 3.20-3.11 (m, 4H), 1.49-1.43 (m, 4H), 1.32-1.24 (m, 12H). ^{13}C-NMR ($CDCl_3$, 100 MHz): 156.50, 136.75, 128.35, 128.20, 128.16, 71.99, 70.66, 70.61, 70.57, 69.75, 66.62, 63.86, 59.06, 41.18, 41.10, 30.00, 29.48, 29.28, 26.78. LC-MS: t = 8.09 min, m/z: 541.33 $[M+H]^+$. MALDI-TOF-MS: m/z calc: 540.34, found: 562.82 $[M+Na]^+$.

Compound 7d

Yield: 1.70 g, 48%. ^{1}H-NMR ($CDCl_3$, 400 MHz): 7.35-7.27 (m, 5H), 5.08 (s, 2H), 4.87 (br s, 1H), 4.77 (br s, 1H), 4.21-4.18 (m, 2H), 3.70-3.61 (m, 12H), 3.54-3.52 (m, 2H), 3.37 (s, 3H), 3.19-3.10 (m, 4H), 1.48-1.43 (m, 4H), 1.26-1.23 (m, 16H). ^{13}C-NMR

($CDCl_3$, 100 MHz): 156.53, 136.78, 129.01, 128.61, 128.18, 72.02, 70.70, 70.64, 70.60, 69.79, 66.66, 63.89, 59.13, 41.22, 41.14, 30.04, 29.60, 29.35, 26.83. LC-MS: t = 8.80 min, 569.40 m/z: $[M+H]^+$. MALDI-TOF-MS: m/z calc: 568.37, found: 590.87 $[M+Na]^+$.

Synthesis of compounds 8a-d

Compound **7a**-**d** (**7a**: 1.33 g, 2.75 mmol; **7b**: 1.74 g, 3.40 mmol; **7c**: 1.14 g, 2.11 mmol; **7d**: 1.17 g, 2.05 mmol) was dissolved in anhydrous MeOH (10 mL), and Pd/C (**a**: 29.80 mg, 0.28 mmol; **b**: 36.18 mg, 0.34 mmol; **c**: 22.35 mg, 0.21 mmol; **d**: 22.35 mg, 0.21 mmol) was added. The solution was degassed with nitrogen, prior to the dropwise addition of triethylsilane (**a**: 4.4 mL, 27.50 mmol; **b**: 5.4 mL, 34.00 mmol; **c**: 3.4 mL, 21.10 mmol; **d**: 3.3 mL, 20.50 mmol). The addition of triethylsilane resulted in the formation of an effervescent solution and once the reaction was complete (as demonstrated by TLC), the solution was filtered through Celite to remove the remaining Pd/C. The filtrate was concentrated by rotary evaporation and afterwards, a gentle stream of nitrogen gas. The dried product was redissolved in CH_2Cl_2 (15 mL). 3,4-Dibutoxy-3-cyclobutene-1,2-dione (**a**: 0.65 mL, 3.03 mmol; **b**: 0.81 mL, 3.74 mmol; **c**: 0.50 mL, 2.32 mmol; **d**: 0.49 mL, 2.26 mmol) and DIPEA (**a**: 0.95 mL, 5.50 mmol; **b**: 1.1 mL, 6.80 mmol; **c**: 0.74 mL, 4.22 mmol; **d**: 0.71 mL, 4.10 mmol) were added to the reaction mixture and stirred at room temperature overnight. Subsequently, CH_2Cl_2 (15 mL) was added and washed with H_2O (30 mL). The aqueous fractions were back-extracted 3x with CH_2Cl_2 (3 x 30 mL). The organic fractions were combined and dried with $MgSO_4$, prior to removing the solvent in vacuo. The crude product was further purified by silica gel column chromatography using a CH_2Cl_2/EtOAc gradient (10-50 vol% EtOAc). The product was concentrated by rotary evaporation to provide an oil (**8a**-**d**) that was further dried in a vacuum oven overnight.

Compound 8a

Yield: 1.09 g, 73%. ^{1}H-NMR ($CDCl_3$, 400 MHz): 5.14 (br s, 1H), 4.71-4.68 (m, 2H), 4.17-4.15 (m, 2H), 3.64-3.59 (m, 12H), 3.52-3.50 (m, 2H), 3.38-3.35 (m, 2H), 3.33 (s, 3H), 3.14-3.09 (q, 2H), 1.76-1.71 (m, 2H), 1.59-1.56 (m, 2H), 1.47-1.30 (m, 8H), 0.95-0.89 (m, 3H). ^{13}C-NMR ($CDCl_3$, 100 MHz): 189.71, 182.75, 177.52, 172.47, 156.64, 73.45, 71.87, 70.54, 70.49, 70.46, 70.43, 69.62, 63.82, 58.99, 44.65, 40.70, 32.03, 30.43, 29.77, 26.10, 25.90, 18.67, 13.70. LC-MS: t = 6.20 min, 503.20 m/z $[M+H]^+$. MALDI-TOF-MS: m/z calc: 502.29, found: 524.81 $[M+Na]^+$.

Compound 8b

Yield: 1.23 g, 68%. ^{1}H-NMR ($CDCl_3$, 400 MHz): 7.47 (br s, 1H), 5.10 (br s, 1H), 4.60-4.57 (m, 2H), 4.08-4.03 (m, 2H), 3.53-3.48 (m, 12H), 3.41-3.39 (m, 2H), 3.30-3.24 (m, 2H), 3.22 (s, 3H), 3.01-2.96 (q, 2H), 1.66-1.60 (m, 2H), 1.48-1.45 (m, 2H), 1.35-1.16 (m, 12H), 0.840.78 (m, 3H). ^{13}C-NMR ($CDCl_3$, 100 MHz): 189.33, 182.88, 176.97, 172.30, 156.27, 72.99, 72.84, 71.57, 70.23, 70.19, 70.16, 70.12, 69.30, 63.47, 58.66, 44.52, 40.64, 31.72, 30.29, 29.57, 28.81, 28.73, 26.32, 26.02, 18.37, 13.41. LC-MS: t = 6.83 min, m/z: 531.33 $[M+H]^+$. MALDI-TOF-MS: m/z calc: 530.32, found: 552.87 $[M+Na]^+$.

Compound 8c

Yield: 0.81 g, 69%. ^{1}H-NMR ($CDCl_3$, 400 MHz): 6.59 (br s, 1H), 4.91 (br s, 1H), 4.74-4.71 (m, 2H), 4.20-4.18 (m, 2H), 3.67-3.62 (m, 12H), 3.55-3.52 (m, 2H), 3.41-3.36 (m, 2H), 3.36 (s, 3H), 3.16-3.11 (q, 2H), 1.79-1.75 (m, 2H), 1.61-1.57 (m, 2H), 1.48-1.26 (m, 16H), 0.97-0.94 (m, 3H). ^{13}C-NMR ($CDCl_3$, 100 MHz): 189.77, 182.84, 177.42, 172.66, 156.63, 73.42, 72.02, 70.68, 70.63, 70.61, 70.58, 69.75, 63.91, 59.11, 44.99, 41.13, 32.15, 30.77, 30.04, 29.53, 29.34, 29.23, 26.83, 26.50, 18.80, 13.83. LC-MS: t = 7.60 min, m/z: 559.27 $[M+H]^+$. MALDI-TOF-MS: m/z calc: 558.35, found: 580.91 $[M+Na]^+$.

Compound 8d

Yield: 0.62 g, 52%. ^{1}H-NMR ($CDCl_3$, 400 MHz): 6.23 (br s, 1H), 4.87 (br s, 1H), 4.75-4.67 (m, 2H), 4.21-4.19 (m, 2H), 3.68-3.63 (m, 12H), 3.56-3.53 (m, 2H), 3.44-3.41 (m, 2H), 3.37 (s, 3H), 3.17-3.12 (q, 2H), 1.62-1.56 (m, 2H), 1.49-1.25 (m, 22H), 0.98-0.95 (m, 3H). ^{13}C-NMR ($CDCl_3$, 100 MHz): 189.66, 182.70, 177.40, 172.43, 156.40, 73.36, 71.89, 70.56, 70.51, 70.47, 69.66, 63.79, 59.00, 44.89, 41.02, 32.01, 30.66, 29.92, 29.49, 29.45, 29.23, 29.12, 26.72, 26.37, 18.66, 13.68. LC-MS: t = 8.32 min, m/z: 587.27 $[M+H]^+$. MALDI-TOF-MS: m/z calc: 586.38, found: 608.55 $[M+Na]^+$.

Synthesis of compounds 1-5

Compound **8a-d** (**8a**: 0.52 g, 1.04 mmol; **8b**: 0.49 g, 0.92 mmol; **8c**: 0.64 g, 1.15 mmol; **8d**: 0.32 g, 0.54 mmol) was dissolved in $CHCl_3$ (15 mL). Tris(2-aminoethyl)amine (**a**: 46 µL, 0.31 mmol; **b**: 40 µL, 0.27 mmol; **c**: 52 µL, 0.35 mmol; **d**: 24 µL, 0.16 mmol) and DIPEA (**a**: 181 µL, 1.04 mmol; **b**: 160 µL, 0.92 mmol; **c**:

200 µL, 1.15 mmol; **d**: 94 µL, 0.54 mmol) were added to the reaction mixture. The solution was refluxed overnight and purified by flash column chromatography on a C18 silica gel column using a gradient of 10-90% CH_3CN/H_2O over 35 minutes. The product was concentrated by rotary evaporation and lyophilized. The compounds were further purified by HPLC with UV detection and lyophilized to obtain the white compounds **1-4**. For the synthesis of compound **5**, tris(2-aminoethyl) amine (12 µL, 0.08 mmol) was dissolved in water (5 mL) and stirred on an ice bath. Subsequently, 1,1'-carbonyldiimidazole (40 mg, 0.25 mmol) was added to the reaction mixture and stirred for 30 minutes. Another identical amount of 1,1'-carbonyldiimidazole was added and the reaction was stirred for another 30 minutes on an ice bath. Once the reaction was complete (as demonstrated by TLC-MS), the aqueous solution was lyophilized overnight and redissolved in $CHCl_3$. The hydrogenated compound **7e** (107 mg, 0.26 mmol) derived from **7c** and DIPEA (45 µL, 0.26 mmol) were added to the reaction mixture and refluxed overnight. The product was purified by HPLC using mass detection and lyophilized overnight to obtain a white solid **5**.

Compound 1

Yield: 0.22 g, 51%. ^{1}H-NMR (DMSO-d_6, 400 MHz): 7.46 (br s, 3H), 7.27 (br s, 3H), 7.18 (br s, 3H), 4.03-4.01 (m, 6H), 3.55-3.40 (m, 54H), 3.23 (s, 9H), 2.96-2.93 (m, 6H), 2.70-2.68 (m, 6H), 1.49-1.26 (m, 24H). ^{13}C-NMR (DMSO-d_6, 100 MHz): 182.65, 168.27, 167.77, 156.42, 71.54, 70.07, 70.03, 69.98, 69.84, 69.16, 63.27, 58.31, 54.96, 43.53, 41.83, 40.40, 30.96, 29.57, 26.13, 25.85. LC-MS: t = 5.14 min, *m/z*: 1431.87 $[M+H]^+$. MALDI-TOF-MS: m/z calc: 1430.80, found: 1452.69 $[M+Na]^+$.

Compound 2

Yield: 0.22 g, 54%. ^{1}H-NMR (DMSO-d_6, 400 MHz): 7.53 (br s, 3H), 7.34 (br s, 3H), 7.14 (br s, 3H), 4.04-4.01 (m, 6H), 3.58-3.40 (m, 54H), 3.23 (s, 9H), 2.96-2.91 (m, 6H), 2.73 (s, 6H), 1.53-1.21 (m, 36H). ^{13}C-NMR (DMSO-d_6, 100 MHz): 182.63, 168.28, 167.71, 156.45, 71.61, 70.14, 70.11, 70.07, 69.91, 69.25, 63.32, 58.30, 55.05, 43.66, 41.60, 40.52, 31.05, 29.98, 29.72, 29.08, 29.02, 26.60, 26.21. LC-MS: t = 5.93 min, m/z: 1515.67 $[M+H]^+$. MALDITOF-MS: *m/z* calc: 1514.81, found: 1536.80 $[M+Na]^+$.

Compound 3

Yield: 0.30 g, 52%. ^{1}H-NMR (DMSO-d_6, 400 MHz): 7.49 (br s, 3H), 7.30 (br s, 3H), 7.18 (br s, 3H), 4.04-4.02 (m, 6H), 3.56-3.38 (m, 54H), 3.24 (s, 9H), 2.96-2.91 (q, 6H), 2.69 (s, 6H), 1.49-1.23 (m, 48H). ^{13}C-NMR (DMSO-d_6, 100 MHz): 182.59, 168.23, 167.68, 156.36, 71.52, 70.05, 70.02, 69.96, 69.82, 69.15, 63.22, 58.29, 54.97, 43.55, 41.63, 40.44, 30.97, 29.66, 29.28, 29.25, 29.02, 28.94, 26.53, 26.15. LC-MS: t = 6.89 min, m/z: 1599.87 $[M+H]^+$. MALDI-TOF-MS: m/z calc: 1598.99, found: 1622.42 $[M+Na]^+$.

Compound 4

Yield: 0.11 g, 42%. ^{1}H-NMR (DMSO-d_6, 400 MHz): 7.61 (br s, 3H), 7.45 (br s, 3H), 7.16 (br s, 3H), 4.03-4.01 (m, 6H), 3.57-3.40 (m, 54), 3.23 (s, 9H), 2.95-2.90 (q, 6H), 2.64 (s, 6H), 1.51-1.21 (m, 60H). ^{13}C-NMR (DMSO-d_6, 100 MHz): 182.40, 182.27, 168.03, 167.45, 156.17, 71.33, 69.86, 69.83, 69.78, 69.64, 68.96, 63.03, 58.09, 54.80, 43.38, 41.43, 40.25, 30.76, 29.47, 29.14, 29.12, 28.86, 28.77, 26.35, 25.96. LC-MS: t = 7.81 min, m/z: 1684.73 $[M+H]^+$. MALDI-TOF-MS: m/z calc: 1683.08, found: 1706.45 $[M+Na]^+$.

Compound 5

Yield: 0.065 g, 56%. ^{1}H-NMR (DMSO-d_6, 400 MHz): 7.19-7.16 (m, 3H), 6.21 (br s, 6H), 4.04-4.01 (m, 6H), 3.55-3.41 (m, 54H), 3.23 (s, 9H), 2.98-2.90 (m, 12H), 1.38-1.22 (m, 48H). ^{13}C-NMR (DMSO-d_6, 100 MHz): 158.87, 156.40, 71.54, 70.07, 70.04, 69.98, 69.84, 69.17, 63.25, 58.31, 54.46, 40.47, 30.17, 29.68, 29.33, 29.30, 29.14, 29.05, 26.74, 26.55. LC-MS: t = 6.86 min, m/z: 1443.5 $[M+H]^+$. MALDI-TOF-MS: *m/z* calc: 1443.0, found: 1444.43 $[M+H]^+$.

2.6.3 Gel inversion tests and critical gelation concentration (CGC) determination

The CGC is defined as the minimum concentration of a given molecule to form a gel. The CGC of molecule **2** was determined by dissolving 2.5 mg (V_1), 3.0 mg (V_2), 3.5 mg (V_3), 4.0 mg (V_4), 4.5 mg (V_5) and 5.0 mg (V_6) of **2** in 500 µL of deionized water in glass vials (2 mL) to various concentrations. All samples were sonicated on a Branson 2510 Ultrasonic Cleaner bath at room temperature for 20 minutes at 298 K and left to stand overnight.

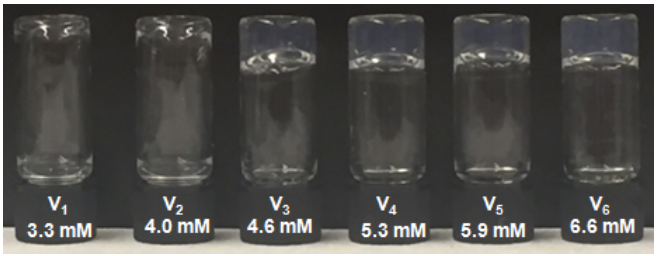

Figure S2.1 Gel inversion test of compound **2**.

The CGC of molecule **3** was also determined by dissolving 0.5 mg (V_1), 1.0 mg (V_2), 1.5 mg (V_3), 2.0 mg (V_4) and 2.5 mg (V_5) of **3** in 500 µL deionized water in a separate glass vial (2 mL) to various concentrations. All samples were sonicated on a Branson 2510 Ultrasonic Cleaner bath at room temperature for 20 minutes at 298 K.

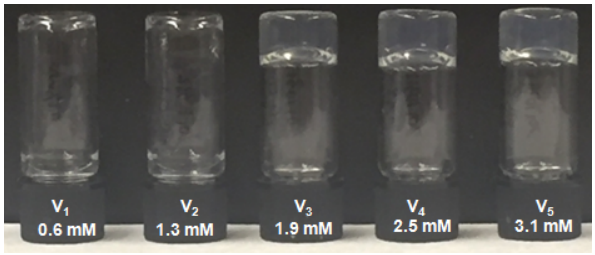

Figure S2.2 Gel inversion test of compound **3**.

2.6.4 Oscillatory rheology

Hydrogels **2** (800 µL, 5.6 mM) and **3** (800 µL, 3.1 mM) in deionized water or in PBS (pH 7.4) were prepared by sonication for 20 min and left to stand overnight before being pipetted onto the lower plate of the rheometer. All time sweep measurements were performed at a frequency (f) of 1.0 Hz with 0.05% strain. Frequency sweeps were conducted in the range of 0.01-2.0 Hz with 0.05% strain. Strain sweeps were measured in the range of 0.001-300% strain for hydrogel **2** and 0.001-100% for hydrogel **3** at a constant frequency of 1.0 Hz. Prior to measuring self-recovery of the supramolecular materials, a time sweep measurement was performed first (f = 1.0 Hz, γ = 0.05%) followed by a frequency sweep (f = 0.01 to 2.0 Hz, γ = 0.05%). Once a plateau in the storage modulus (G') was reached, a strain of 200% for hydrogel **2** and 100% strain for hydrogel **3** was applied for 120 s. The gel was then allowed to recover while measuring at 0.05% strain and continued with a frequency sweep (from 0.01 to 2.0 Hz, γ = 0.05%) back

to the original plateau of the storage modulus. The strain was alternated in this manner for two cycles.

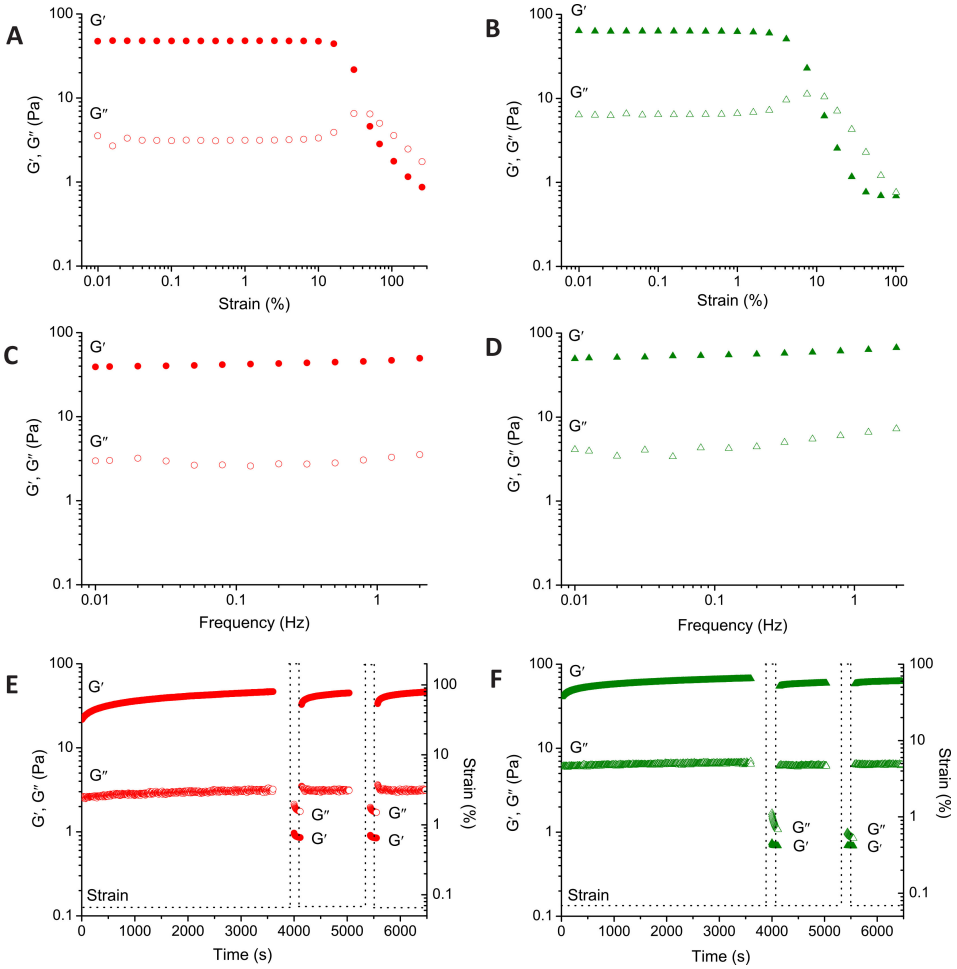

Figure S2.3 Oscillatory rheology measurements of hydrogels **2** (5.6 mM) and **3** (3.1 mM) in deionized water at 25 °C: Amplitude sweep (1.0 Hz) for hydrogels **2** (A) and **3** (B). Frequency sweep (0.05% strain) of hydrogels **2** (C) and **3** (D). Step strain measurements (1.0 Hz) for hydrogels **2** (E) and **3** (F), the absence of data between the application of high strain is due to the acquisition of a frequency sweep (from 0.01 to 2.0 Hz, γ = 0.05%).

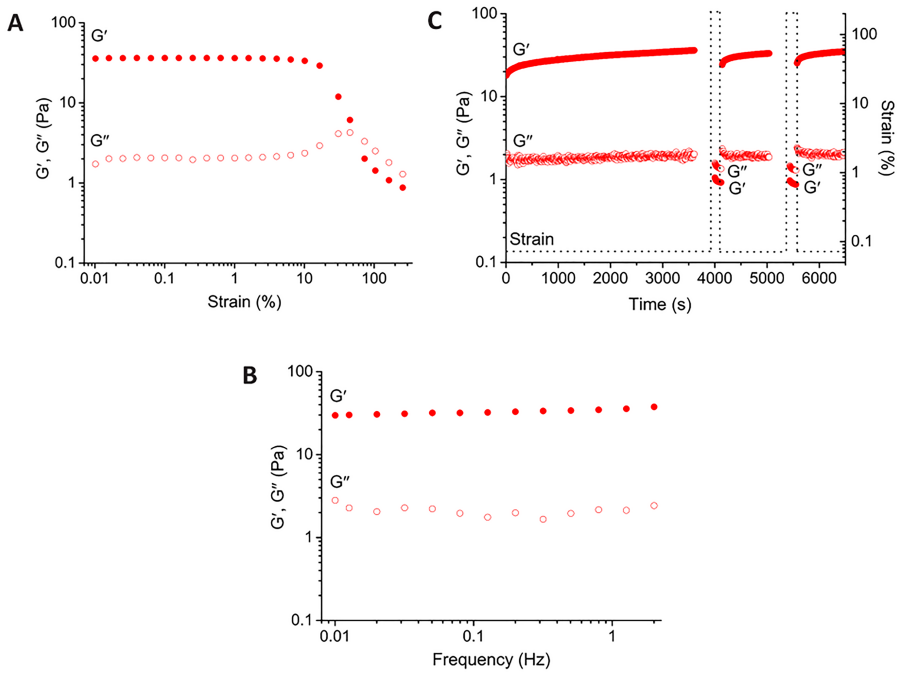

Figure S2.4 Oscillatory rheology measurements of the hydrogel **2** (5.6 mM) in PBS at 37 °C: (A) Amplitude sweep (f = 1.0 Hz). (B) Frequency sweep (γ = 0.05%). (C) Step strain measurements (f = 1.0 Hz). The absence of data before the application of high strain is due to the acquisition of a frequency sweep (from 0.01 to 2.0 Hz, γ = 0.05%).

2.6.5 Cryo-electron microscopy (cryo-TEM)

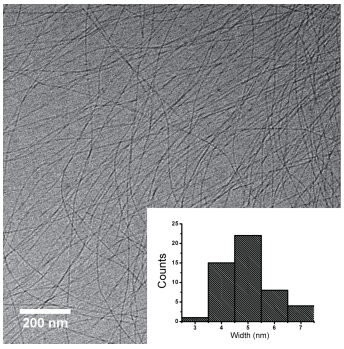

Figure S2.5 Cryo-TEM image of hydrogel **2** (5.6 mM) prepared by 20 minutes sonication in an ultrasonic bath and left to stand overnight. Insert: Histograms of width distribution of the fibers for a sample size of N = 50.

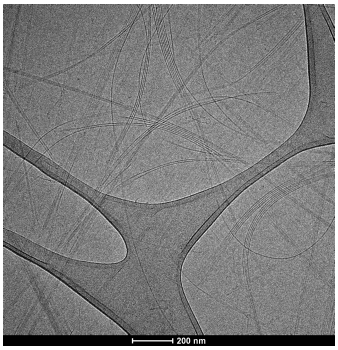

Figure S2.6 Cryo-TEM image of a solution **5** (3.1 mM) in deionized water prepared by 20 minutes sonication in an ultrasonic bath and left to stand overnight.

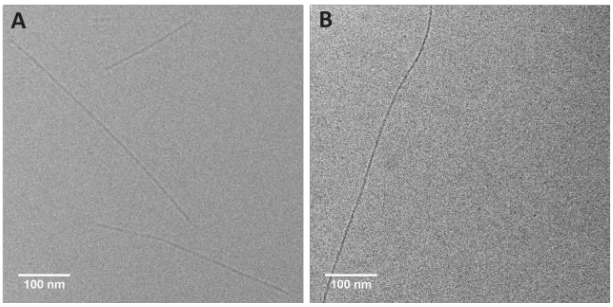

Figure S2.7 (A) Cryo-TEM image of a diluted solution of **2** (1.5×10^{-5} M) in deionized water and (B) diluted solution of **3** (1.5×10^{-5} M) prepared by 20 minutes sonication in an ultrasonic bath and left to stand overnight.

2.6.6 Small angle X-ray Scattering (SAXS)

SAXS measurements of monomer **3** (2.0 mg/mL) in deionized water were prepared by sonication of the sample for 20 min in an ultrasonic bath and left to stand overnight at room temperature before pipetting into 2 mm quartz capillaries (Hilgenberg GmbH).

The experimental SAXS profile and the form factor model to describe it is given in **Figure 2.2F** and **Figure S2.8**. In the low-*q* regime the scattering profiles decay with a powerlaw slope of approximate unity, which is typical for one-dimensional objects. The experimental data was modelled using a form factor developed for flexible cylinders, with a fixed $\rho_{solvent} = 9.37 \cdot 10^6$ A^{-2}. From the model, we obtain values for the cross-sectional radius of the fibers, r_{cs}, their electron length density, ρ_{cyl}, and kuhn length, l_K (see **Table S2.1**). Several form factors were tested, including those of stiff homogeneous and flexible homogeneous cylinders (the latest best describe the data and was therefore selected). The slope in the

low *q*-regime showed a value of 1.71 (**Figure S2.8**) and it was used for the determination of the $I_{cs}(q)$ (**Figure S2.9**). We extract the cross-sectional mass per unit length, M_L, from the height of the $I_{cs}(q)$ plateau according to

$$\frac{d\Sigma(q)}{d\Omega} = I(q) = \frac{\pi}{q} I_{cs}(q) \tag{1}$$

$$M_L = \frac{I_{cs}(0)}{c\Delta\rho_M^2} \tag{2}$$

with the electron length density difference per mass, $\Delta\rho_M$ (extracted from the fitting curves in SasView, where $\Delta\rho_M = \Delta(\rho_{cyl}-\rho_{solv})$.

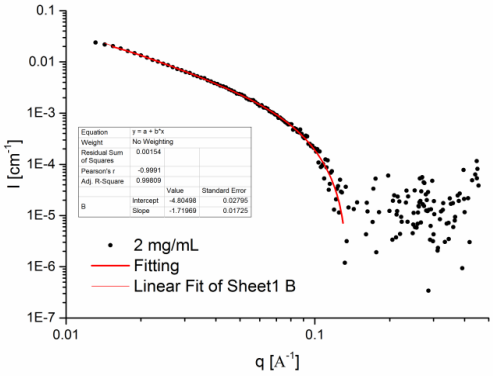

Figure S2.8 Scattering profile of **3** (2.0 mg mL^{-1}). Black dots represent experimental data; the red line represents form a factor model for flexible cylinders. The slope was determined to be ~1.71 in the low *q*-regime (*blue line*).

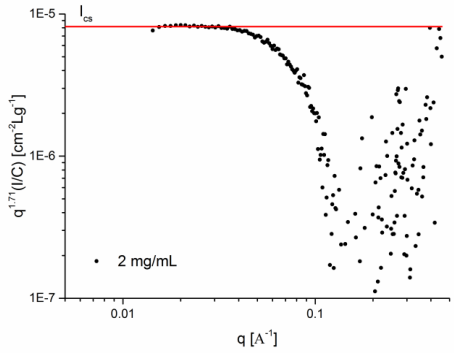

Figure S2.9 $I_{cs}(q)$ determination plot of the scattering profile in **Figure 2.2F**. The $I_{cs}(q)$ plateau ($0.0143 \leq q \leq 0.0383$ Å^{-1}) is indicated by a red line.

Table S2.1 Structural parameters extracted from Holtzer representation of SAXS profiles.

Sample	$\Delta\rho_{cyl}$ ($Å^{-2}$)	$\Delta\rho_{sol}$ ($Å^{-2}$)	$\Delta\rho_{M}$ ($cm\ g^{-1}$)	I ($cm^{-2}\ L\ g^{-1}$)	I_{cs} (0) (cm^{-2})	M_L (g/nm)	Molec/nm	R_{cs} (nm)	Kuhn L (nm)
2 mg/mL	9.04×10^{6}	9.37×10^{6}	3.27×10^{9}	8.15×10^{2}	1.04×10^{3}	2.42×10^{-21}	0.92	2.608	6.591

2.6.7 UV-Vis Spectroscopy

Stock solutions of **2** and **3** in deionized water (1.5 mM) were prepared separately with 20 min sonication in an ultrasonic bath and were subsequently diluted to their measured concentrations. The individual samples were left to stand overnight at room temperature prior to measurements.

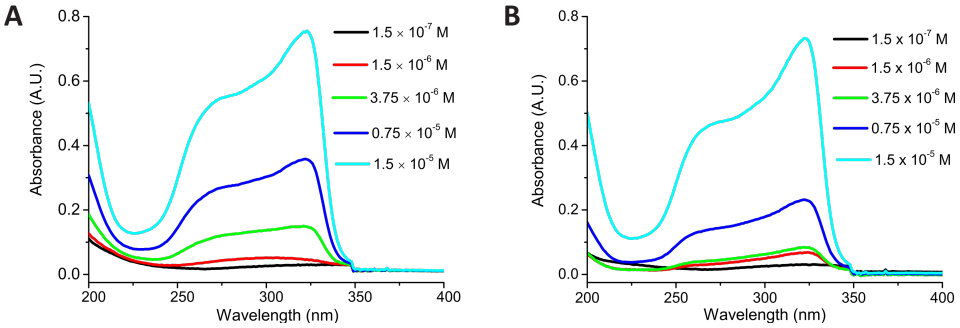

Figure S2.10 Concentration-dependent UV-Vis spectra of **2** (A) and **3** (B) in deionized water.

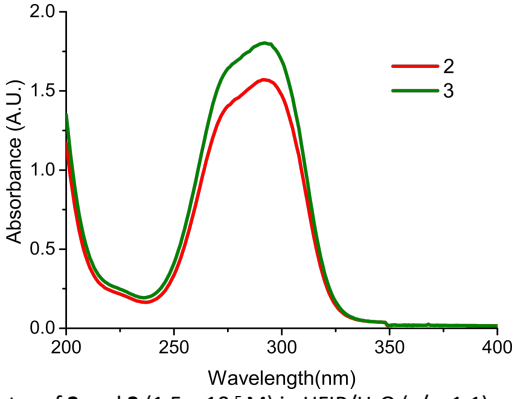

Figure S2.11 UV-Vis spectra of **2** and **3** (1.5×10^{-5} M) in HFIP/H_2O (v/v, 1:1).

2.6.8 Fluorescence Spectroscopy

A stock solution of Nile Red dye in methanol (0.005 mg/mL) was prepared. Aliquots (12 µL) from the Nile Red stock solution were pipetted into the individual wells of a 96-well plate. Subsequently, the methanol was removed by placing the

96-well plate into a vacuum oven for 2 h at room temperature. Stock solutions of **1**-**3** were prepared in deionized water (1.5 mM) with sonication for 20 min in an ultrasonic bath. Aliquots (10 µL) were taken from these stock solutions and diluted in deionized water (990 µL) to obtain the desired concentration (1.5×10^{-5} M). Subsequently, the diluted solutions of **1**-**3** were pipetted into the 96-well plate containing the Nile Red dye and left to stand overnight prior to measurements. As a negative control, the Nile Red dye was also measured in water (200 µL) within the microplate.

2.6.9 Fourier Transform Infrared (FTIR) Spectroscopy

Samples of **1**-**3** were first prepared in deionized water (400 µL, 3.1 mM) in an ultrasonic bath for 20 min and left to stand overnight. The samples were then lyophilized prior to solid FTIR measurements.

Table S2.2 Infrared spectra assignment of vibrational modes from 3700-1500 cm^{-1} for the various peaks indicated in **Figure 2.3C** of freeze-dried samples **1-3**.

	Sample **1**	Sample **2**	Sample **3**
v (N-H)	3317 cm^{-1} (carbamate) 3164 cm^{-1} (squaramide)	3317 cm^{-1} (carbamate) 3165 cm^{-1} (squaramide)	3315 cm^{-1} (carbamate) 3167 cm^{-1} (squaramide)
v (C-H)	2931 cm^{-1} (antisym) 2861 cm^{-1} (sym)	2925 cm^{-1} (antisym) 2854 cm^{-1} (sym)	2918 cm^{-1} (antisym) 2850 cm^{-1} (sym)
v (C=O)	1719 and 1693 cm^{-1} (carbamate) 1654 and 1639 cm^{-1} (squaramide)	1719 and 1692 cm^{-1} (carbamate) 1644 cm^{-1} (squaramide)	1720 and 1689 cm^{-1} (carbamate) 1652cm^{-1} (squaramide)
Ring breathing	1799 cm^{-1}	1799 cm^{-1}	1799 cm^{-1}

2.6.10 Cell Culture

A NIH 3T3 cell line was cultured and maintained in DMEM medium with 10% FBS. A hiPSC line (SFLB6)[3] was maintained on human recombinant vitronectin-coated plates in TeSR-E8 cell culture medium (STEMCELL Technologies). hiPSC-derived endothelial cells (ECs) were cultured on gelatin-coated plates in EC-SFM (Invitrogen) additionally supplemented with 1% platelet-poor serum, 30 ng/mL of VEGF, and 20 ng/mL of bFGF as previously described.[4] For NIH 3T3 cells, 100 units/mL of penicillin and 100 µg/mL of streptomycin were added to the culture media, whereas hiPSCs and hiPSC-derived endothelial cells were cultured in

penicillin/streptomycin-free medium. All cells were cultured in an incubator at 37 °C with a 5% CO_2 atmosphere.

2.6.11 MTT assays

NIH 3T3 cells were seeded at a density of 1500 cells/well in a 96-well plate and allowed to adhere overnight. Aliquots of **1**-**3** were pipetted into the wells to provide final concentrations of 1, 10, 50, 100, and 200 µM in PBS or deionized water and incubated with the cells for 24 and 72 h. Measurements were performed for each condition in triplicate. A 10 µL aliquot of a 3-[4,5-dimethyl-2-thiazolyl]-2,5-diphenyl-2H-tetrazolium bromide (MTT) stock solution (5.0 mg/mL in PBS) was added to each well. After incubation for 2-3 h with MTT, the medium was aspirated, and 200 µL of DMSO was added to dissolve the formazan crystals produced. Cell viability was calculated from the absorbance measured at 570 nm on a fluorescence microplate reader (TECAN).

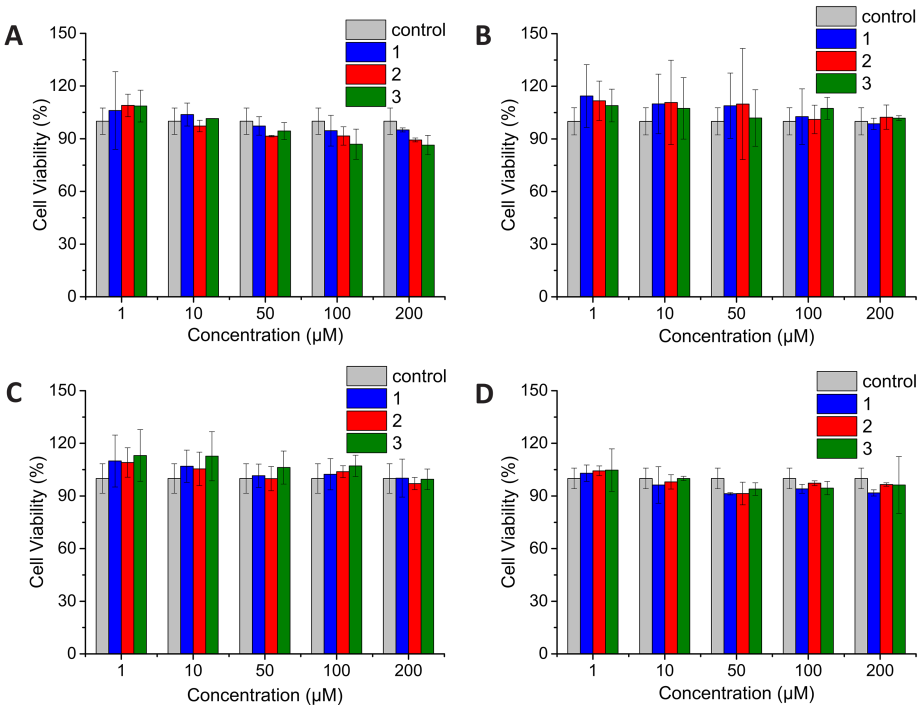

Figure S2.12 Results of the MTT cytotoxicity test for monomers **1**-**3** ranging in concentration (1-200 µM) with NIH 3T3 cells under various conditions (N = 3): (A) in deionized water after 24 h. (B) in deionized water after 72 h. (C) in PBS after 24 h. (D) in PBS after 72 h.

2.6.12 3D cell encapsulation studies

NIH 3T3 cells were harvested and resuspended in PBS at a concentration of 5 × 10^6 cells/mL. The cell suspension (20 μL) was mixed with premade hydrogels of **2** (180 μL PBS, 6.2 mM) or **3** (180 μL PBS, 3.4 mM), resulting in final concentrations of **2** (5.6 mM) and **3** (3.1 mM) after gently pipetting the gels up and down (~10 times). The cell-laden hydrogels (200 μL) were transferred into an 8-well chamber slide by pipetting. After waiting 15 min at room temperature, cell culture media (100 μL) was then layered on top of the hydrogels before placing them in an incubator at 37 °C. LIVE/DEAD (calcein AM/propidium iodide (PI)) staining of the hydrogels was subsequently performed at specific time points. Stock solutions of calcein AM (2.5 mM in DMSO) and PI (1.5 mM in PBS) were prepared and stored at -20 °C; these stock solutions were diluted with PBS to obtain a staining solution containing both dyes at final concentrations of 2 and 1.5 μM, respectively. The medium on top of the hydrogel was removed by pipetting, and the hydrogel was first washed once with PBS (100 μL) before incubation with the staining solution (100 μL) for 30 min at room temperature. Afterward, the excess staining solution was removed, and the hydrogel was washed twice gently with PBS (100 μL). Additional PBS (100 μL) was added, and the hydrogel-encapsulated cells in 3D were imaged on a Zeiss LSM 710 confocal laser scanning microscope equipped with a Zeiss 5× objective. Fluorescent Z-stack images (35 images/per sample) through the gel were acquired at a resolution of 512 × 512 pixels using an excitation wavelength of 488 nm and an emission filter of 519-582 nm for calcein AM, and an excitation wavelength of 532 nm and an emission filter of 615-695 nm for PI. Cell viability was determined by counting the calcein AM-stained green cells (*viable*) and PI-stained red cells (*dead*) in ImageJ. Z-stack images of 3D cell-laden hydrogels **2** and **3** were taken after 2 and 48 h, respectively. For each hydrogel sample at each time point, five Z-stack images were counted totaling more than 400 cells.

hiPSC-derived ECs and hiPSCs and were dissociated to single cells using 1× TrypLE Select, and the cells were encapsulated in a hydrogel of **3** in 3D using a similar procedure as described earlier for the NIH 3T3 cells. Cell suspensions of hiPSC-derived ECs (5 × 10^6 and 2 × 10^7 cells/mL), and hiPSCs (2 × 10^7 cells/mL) were used for 3D cell seeding within the hydrogels. Aliquots of the various cell suspensions (10 μL) were mixed with premade hydrogels of **3** (90 μL PBS, 3.4 mM) by gentle pipetting to provide a final gel concentration of **3** (3.1 mM). After being left to stand for 15 min at room temperature, 200 μL of cell culture medium was

layered on top of the 3D cell-laden hydrogels. For hiPSCs, TeSR-E8 medium was additionally supplemented with RevitaCell (1:100) when layered on top of the hydrogels, and EGM-2 medium was used for hiPSC-ECs. For the wells containing hiPSCs, the culture medium was refreshed every ~12 h with TeSR-E8. Time-lapse imaging was performed using the EVOS FL AUTO2 system. Z-stack images were acquired with a 10× objective every 15 min for a period from 24 to 72 h. Cell viability was determined using NucGreen Dead reagent (ThermoFisher) after 24 h for both hiPSC and hiPSC-ECs and 72 h for hiPSCs.

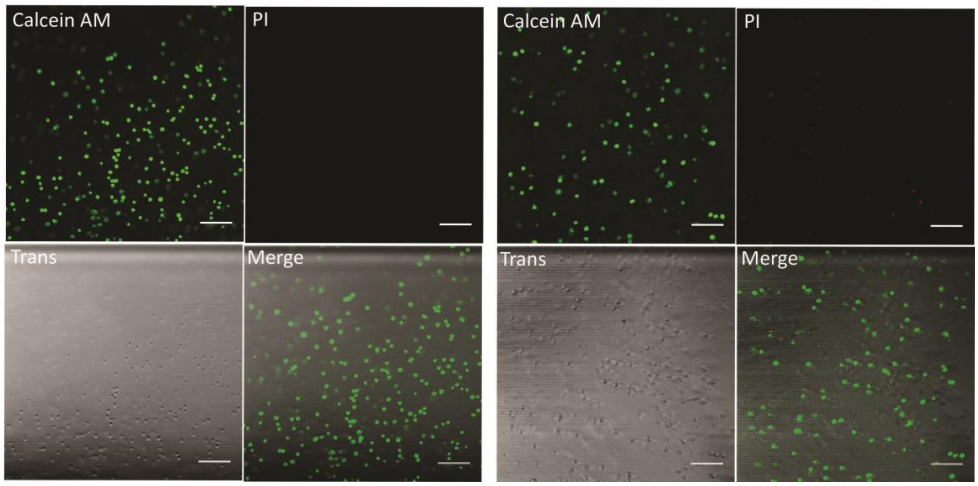

Figure S2.13 Confocal microscopy images of NIH 3T3 cells encapsulated in a hydrogel of **2** (5.6 mM) in 3D: after 2 h incubation (*left*); after 48 h incubation (*right*) (green: *viable cells*, red: *dead cells*). Scale bar: *200 μm*.

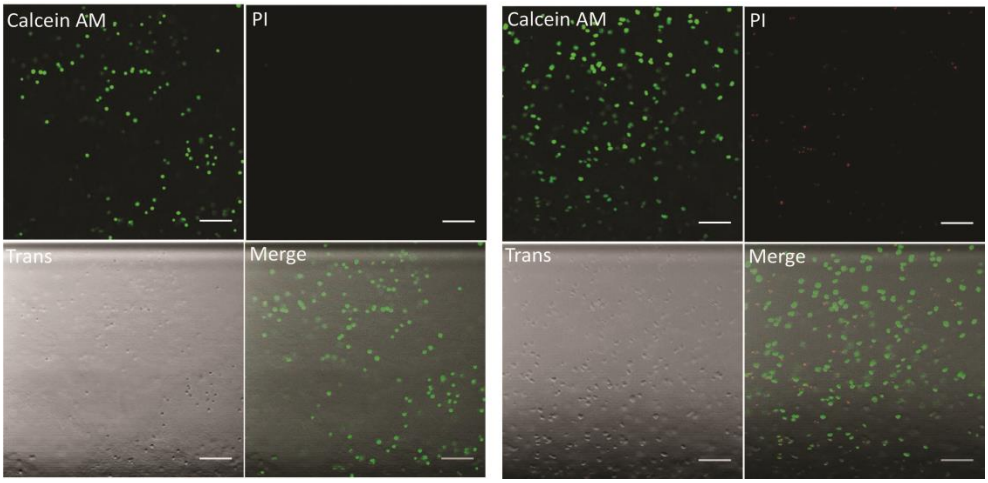

Figure S2.14 Confocal microscopy images of NIH 3T3 cells encapsulated in a hydrogel of **3** (3.1 mM): after 2 h incubation (*left*); after 48 h incubation (*right*) (green: *viable cells*, red: *dead cells*). Scale bar: *200 µm*.

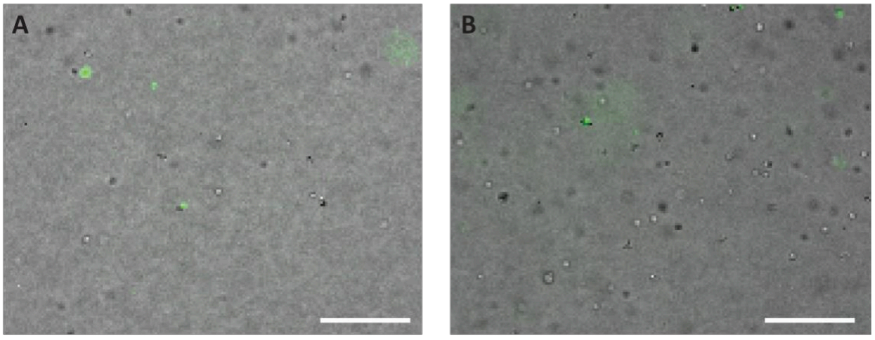

Figure S2.15 3D cell culture of hiPSC-derived ECs encapsulated in the hydrogel **3** (3.1 mM): (A) Representative images of hiPSC-ECs seeded in hydrogel at low density (5×10^6 cells/mL) or (B) high density (2×10^7 cells/mL) and cultured for 24 h. Dead cells were detected using NucGreen® Dead reagent (ThermoFisher). Scale bar: *200 µm*.

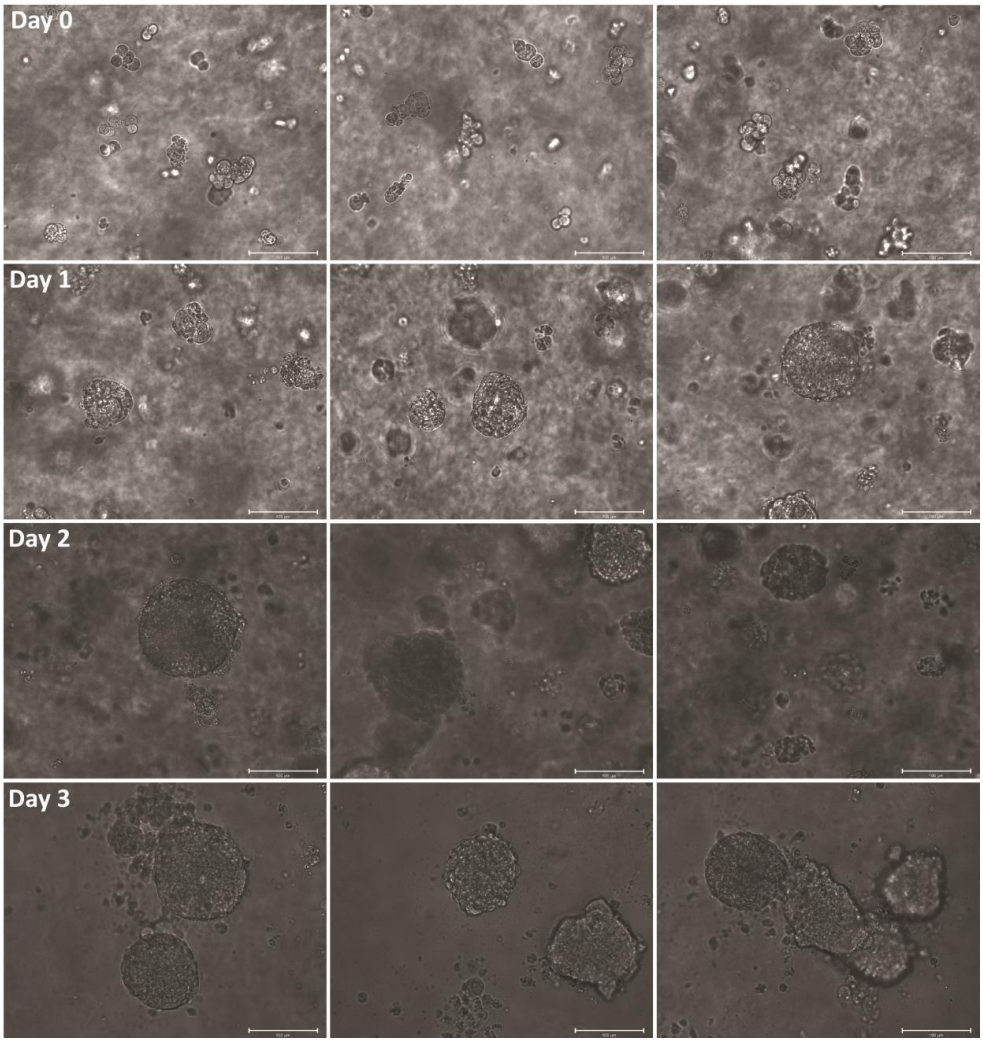

Figure S2.16 Representative images of hiPSCs in hydrogel **3** (3.1 mM) just after seeding, after 24 h, 48 h and 72 h of culture. Scale bar: *100 μm*.

2.6.13 FACS analysis

TRA-1-60-PE and SSEA-4-VioBlue fluorescently labeled antibodies were incubated with the cells at a 1:20 dilution at room temperature and recorded on a MACSQuant VYB flow cytometer with a 561 nm laser for excitation and a 586/15 nm Y1 filter (PE) and 405 nm laser for excitation and a 450/50 nm V1 filter (VioBlue). After 24 h incubation, hiPSCs were released from the hydrogel (100 µL) using gentle mechanical dissociation by pipetting (~15-20 times) from the wells and diluted into 1× PBS (~50× volume). The isolated cell suspension from the gel

was washed 3× times with 1× PBS (3 mL) followed by centrifugation for 3 min at 300g. Cells were dissociated to a single-cell suspension using 1× TrypLE Select, and FACS staining was performed as previously described.[4] hiPSCs cultured on vitronectin-coated plates using standard procedures as described above were used as a positive control in all FACS experiments.

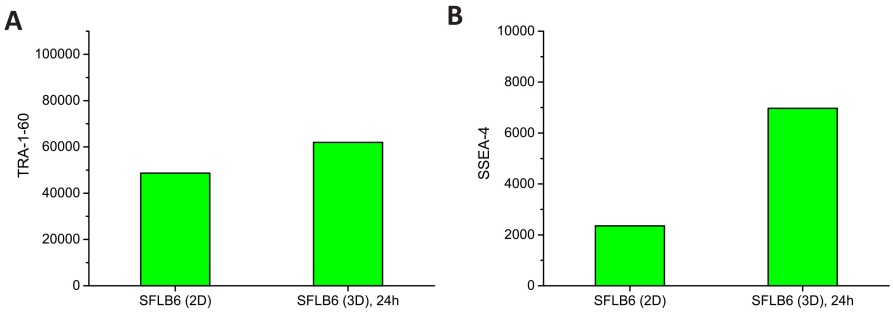

Figure S2.17 3D cell culture of hiPSCs encapsulated in hydrogel **3** (3.1 mM): The values of mean fluorescence intensity (MFI) of the positive cell populations in the expression level of TRA-1-60 (A) and SSEA-4 (B).

2.6.14 References

(1) Kremer, J. R.; Mastronarde, D. N.; McIntosh, J. R. *J. Struct. Biol.* **1996**, *116* (1), 71-76.
(2) Pettersen, E. F.; Goddard, T. D.; Huang, C. C.; Couch, G. S.; Greenblatt, D. M.; Meng, E. C.; Ferrin, T. E. J. *Comput.Chem.* **2004**, *25* (13), 1605-1612.
(3) Zhang, M.; D'Aniello, C.; Verkerk, A. O.; Wrobel, E.; Frank, S.; Ward-vanOostwaard, D.; Piccini, I.; Freund, C.; Rao, J.; Seebohm, G. *Proc. Natl. Acad. Sci. U. S. A.* **2014**, *111* (50), E5383-E5392.
(4) Orlova, V. V.; Van Den Hil, F. E.; Petrus-Reurer, S.; Drabsch, Y.; Ten Dijke, P.; Mummery, C. L. *Nat. Protoc.* **2014**, *9* (6), 1514-1531.